Quaternary Science Reviews 325 (2024) 108484

Contents lists available at ScienceDirect

Quaternary Science Reviews

journal homepage: www.elsevier.com/locate/quascirev

Responses of small mountain glaciers in the Maritime Alps (south-western European Alps) to climatic changes during the Last Glacial Maximum

Lukas Rettig [a,*], Sarah Kamleitner [b], Paolo Mozzi [a], Adriano Ribolini [c], Susan Ivy-Ochs [b], Brice R. Rea [d], Giovanni Monegato [e], Marcus Christl [b], Matteo Spagnolo [d]

[a] Department of Geosciences, University of Padova, Padova, Italy
[b] Laboratory of Ion Beam Physics, ETH Zürich, Zürich, Switzerland
[c] Department of Earth Sciences, University of Pisa, Pisa, Italy
[d] Department of Geography & Environment, School of Geosciences, University of Aberdeen, Aberdeen, United Kingdom
[e] National Research Council of Italy (CNR), Institute of Geosciences and Earth Resources, Padova, Italy

ARTICLE INFO

Handling editor: Dr C. O'Cofaigh

Keywords:
Equilibrium line altitude
Glacial geomorphology
Glacier chronology
Last glacial maximum
Palaeoclimate reconstructions
Quaternary glaciations
Surface exposure dating

ABSTRACT

We present new chronological data and Equilibrium Line Altitude (ELA) information for palaeoglaciers in the Maritime Alps during the Last Glacial Maximum (LGM) and the early deglaciation. Three relatively small catchments were investigated to test if the response of small (1–10 km^2) glaciers to LGM climatic forcing was distinguishable from that of larger glacial systems. Palaeoglacier geometries and ELAs were reconstructed using geomorphological evidence and toolboxes in a geographic information system. Chronological control was provided through ^{10}Be surface exposure dating of erratic boulders located on frontal and lateral moraine ridges. Our data indicate two phases of glacier advance or stabilisation in the Maritime Alps, the first occurring at ca. 25 to 24 ka and the second at ca. 20.5 to 19 ka. This is consistent with ages that have been reported from larger outlet lobes along the south-western Alpine fringe, where the second LGM advance is usually preserved in the form of a recessional moraine. Within the uncertainty of the dating technique, there are no distinguishable differences between the responses of small and large Alpine glaciers to the LGM climate. The reconstructed ELAs for palaeoglaciers in the Maritime Alps indicate a considerable variability, which appears to be linked to differences in received solar radiation, from ca. 1600 m a.s.l. for north-facing cirque glaciers to almost 2000 m a.s.l. for glaciers with a southerly aspect. We argue that such influence of solar radiation needs to be considered when using ELAs for palaeoclimatic inferences at regional scales. The calculated ELAs are up to 450 m higher than those in the northern Apennines or the Corsican mountains, indicating a relatively dry LGM climate on the Italian side of the Maritime Alps.

1. Introduction

Mountain glaciers respond dynamically to climatic changes, as their mass balances and Equilibrium Line Altitudes (ELAs) are controlled by variations in temperature and precipitation (Ohmura et al., 1992; Ohmura and Boettcher, 2018). The response of a glacier to a change in climate, however, can depend on its size and hypsometry. Short and steep mountain glaciers can adjust to a climatic forcing in a matter of a few years to decades (Jóhannesson et al., 1989; Oerlemans, 2007; Raper and Braithwaite, 2009). Larger glacial systems such as ice caps, on the other hand, may take much longer to transfer a change in accumulation into a terminus advance (Jóhannesson, 1986; Paterson, 1994). This has implications for studying glacier fluctuations in a palaeoclimatic context (Kirkbride and Winkler, 2012), with smaller glaciers potentially representing a preferred target to constrain the chronology of past climatic changes (Reuther et al., 2011).

The Last Glacial Maximum (LGM) can be defined as the period between ca. 26.5 and 19 ka, during which globally many glaciers and ice sheets were at their largest extent (Clark et al., 2009). During the LGM, the European Alps (from hereon: the Alps) saw the evolution of a complex palaeoglacier network with ice domes in the inner parts of the Alps that fed large outlet glaciers, some of which advanced beyond the Alpine front (Ehlers and Gibbard, 2004; Bini et al., 2009; Seguinot et al., 2018; Ivy-Ochs et al., 2022; Monegato et al., 2022). The LGM

* Corresponding author.
E-mail address: lukas.rettig@phd.unipd.it (L. Rettig).

https://doi.org/10.1016/j.quascirev.2023.108484
Received 11 September 2023; Received in revised form 15 December 2023; Accepted 20 December 2023
Available online 8 January 2024

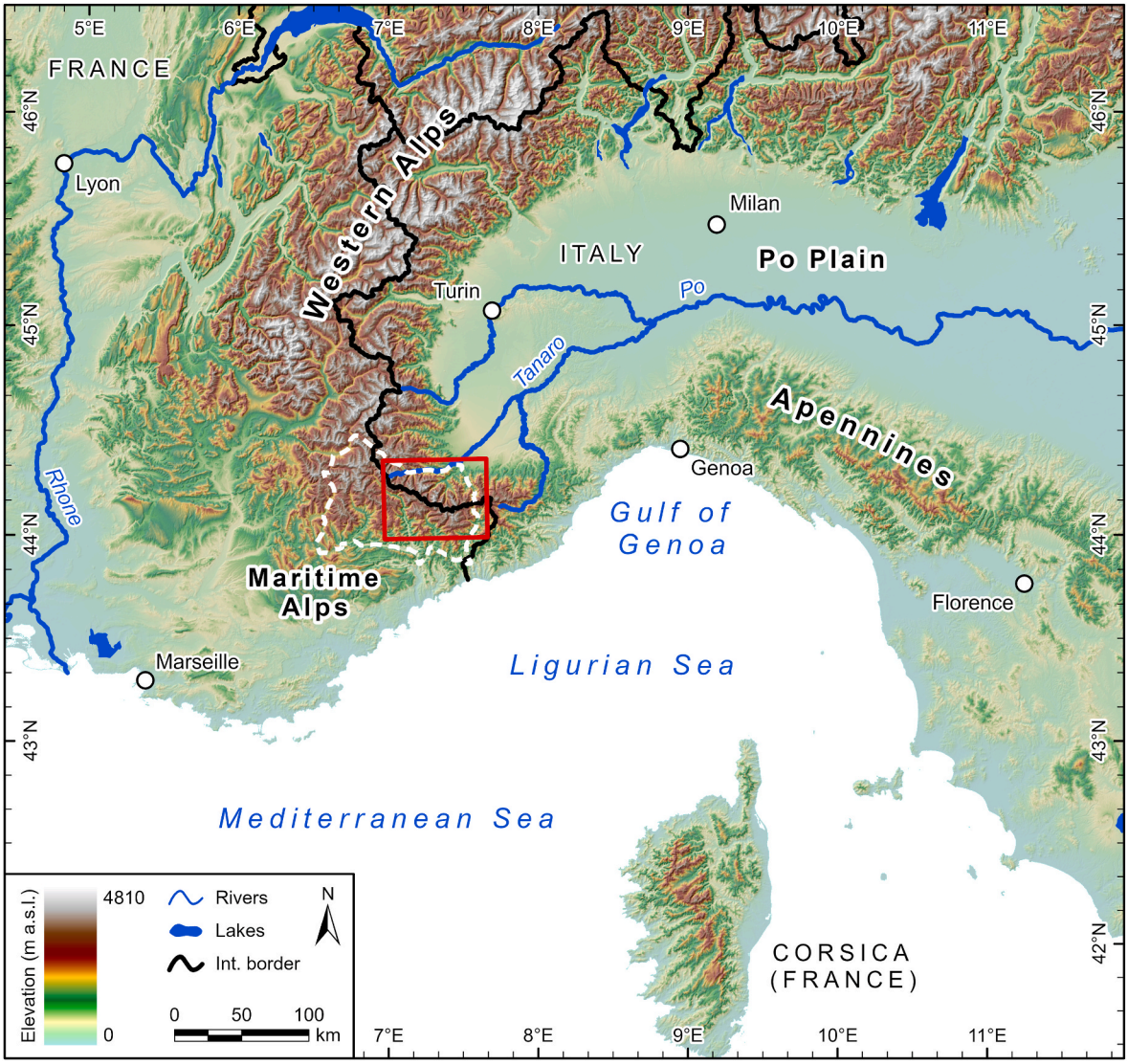

Fig. 1. Location of the Maritime Alps with respect to the western Alpine arc and the Mediterranean Sea. The dashed white line represents the outline of the Maritime Alps according to Marazzi (2005). The extent of Fig. 2 is marked with a red rectangle. Underlying elevation data: EU-DEM v. 1.1. (https://land.copernicus.eu/).

chronology in the Alps is mainly based on the study of end-moraine systems that were built by these advancing glaciers, with surface exposure (Gianotti et al., 2008; Reber et al., 2014; Federici et al., 2017; Ivy-Ochs et al., 2018; Braakhekke et al., 2020; Kamleitner et al., 2022, 2023; Ribolini et al., 2022a; Roattino et al., 2022), radiocarbon (Jorda et al., 2000; Ivy-Ochs et al., 2004; Monegato et al., 2007, 2017; Ravazzi et al., 2012), or luminescence dating (Preusser et al., 2007; Gaar et al., 2019; Gribenski et al., 2021), providing absolute age control. These studies have demonstrated that, with few exceptions (e.g., Gribenski et al., 2021), glaciers across the Alps reached their maximum extent between ca. 28 and 19 ka, in line with the global LGM during Marine Isotope Stage (MIS) 2.

Smaller valley glaciers and ice caps also existed marginal relative to the largest ice masses, such as in the pre-Alpine mountains along the southern fringe of the Alps (Baratto et al., 2003; Forno et al., 2010; Monegato, 2012; Rettig et al., 2021, 2023). The geomorphological evidence (i.e., lateral and frontal moraines) related to these marginal glaciers contains important palaeoclimatic information, as it can be used to reconstruct palaeoglacier 3D-geometries and ELAs (Pellitero et al., 2015, 2016), the latter providing quantitative information on temperature and precipitation at the time of moraine formation (e.g., Chandler and Lukas, 2017; Rea et al., 2020; Rettig et al., 2023). So far, however, moraines in the pre-Alpine mountains along the southern Alpine fringe have been attributed to the LGM only through stratigraphical and morphological means. Due to the lack of absolute age control, it has remained unclear if marginal glaciers responded synchronously to the larger Alpine outlet lobes, or if they adjusted more rapidly to changes in the LGM climatic forcing, as it is suggested by data from the northern face of the Alps (Reuther et al., 2011). A systematic comparison between the chronologies of large and small Alpine palaeoglaciers in a defined geographical area remains to be tested.

The Maritime Alps are located at the south-westernmost end of the Alpine arc (Fig. 1). As a result of their geographic location, close to the Gulf of Genoa, the climate in this region is influenced not only by westerly circulation but also by cyclogenesis in the Mediterranean Sea (Ribolini et al., 2022a), which was likely a key driver for the evolution of LGM glaciation in the Alps (Florineth and Schlüchter, 2000; Luetscher et al., 2015; Monegato et al., 2017; Kamleitner et al., 2022). A better understanding of the chronology and ELAs of palaeoglaciers in the Maritime Alps can therefore also help to decipher the regional LGM climate and precipitation patterns.

The aims of this study are: (1) to constrain glacier advances in three small catchments across the Maritime Alps by means of ^{10}Be surface exposure dating, strengthening the regional LGM chronology; (2) to evaluate if smaller glaciers reacted to the LGM climate forcing in the same way/at the same time as did larger glacial systems in the south-western Alps; and (3) to reconstruct the 3D-geometries and ELAs of these glaciers to gain further insights into the LGM climate in the Alpine and Mediterranean regions.

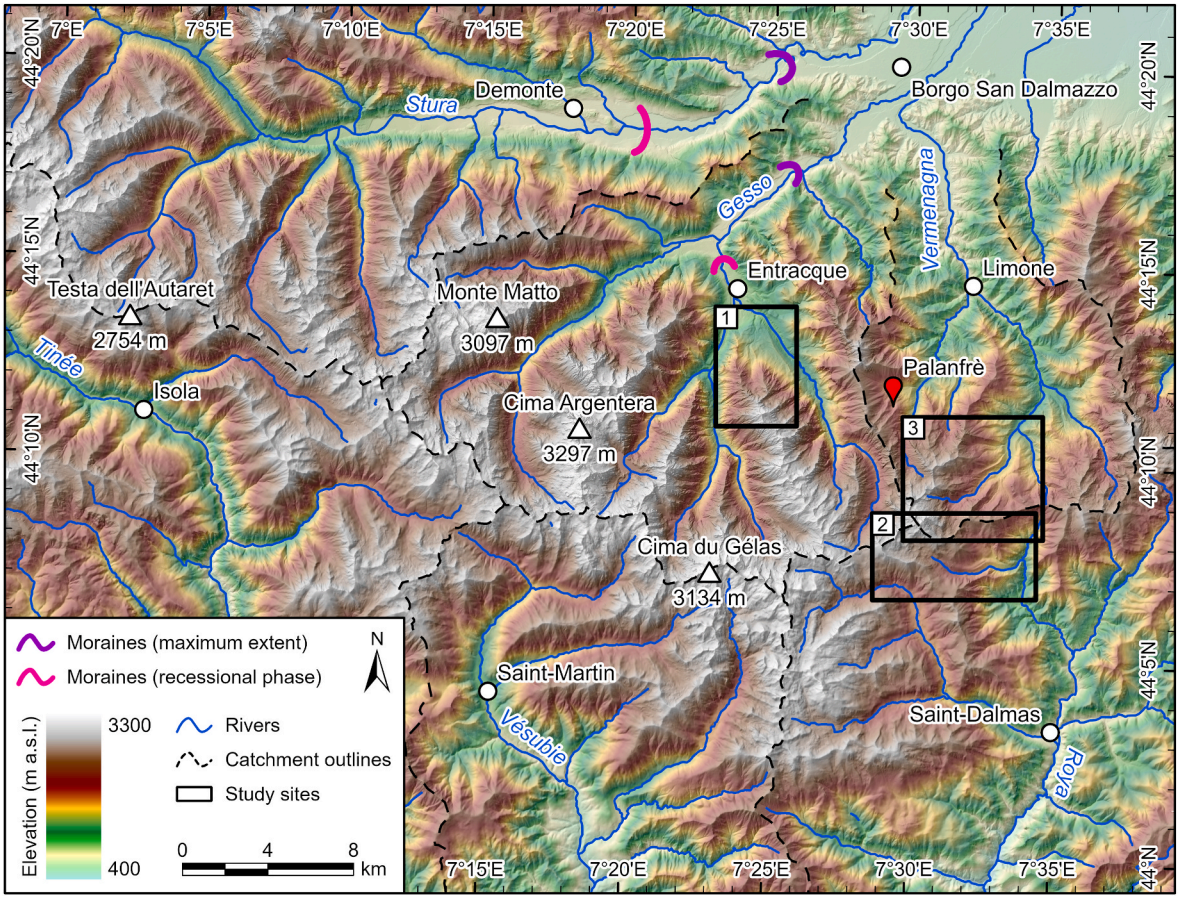

Fig. 2. Topographic map of the north-eastern part of the Maritime Alps. In the Gesso and Stura valleys, the positions of moraine ridges, related to the LGM maximum extent (ca. 25 to 24 ka) and a late LGM recessional phase (ca. 19 ka), are indicated following Federici et al. (2012, 2017), and Ribolini et al. (2022a). The black rectangles refer to the extents of the geomorphological maps for the present study sites: (1) Costa Ganola (Fig. 3), (2) Caramagne (Fig. 4), and (3) Limonetto (Fig. 5). The location of the Palanfrè weather station (for reference meteorological data) is also indicated. Underlying elevation data: RIPRESA AEREA ICE 2009–2011 - DTM 5 (https://www.geoportale.piemonte.it/cms/) and RGE ALTI DTM (https://geoservices.ign.fr/).

2. Study area

2.1. Geographical overview

The Maritime Alps (Italian: *Alpi Marittime*; French: *Alpes Maritimes*) represent the south-westernmost extent of the European Alps (Fig. 1). Their main divide follows the border between the Italian region of Piemonte and the French department of Alpes-Maritimes and reaches elevations of over 3000 m a.s.l. (highest peak: Cima Argentera, 3297 m a.s.l.). The Maritime Alps represent the watershed between the tributaries of the Tanaro River and the upper Po Plain in the north (draining towards the Adriatic Sea) and the Ligurian Sea (Gulf of Genoa) in the south. The northern (Italian) side comprises three main fluvial catchments (Fig. 2): the Stura di Demonte Valley (from hereon: Stura Valley), the Gesso Valley, and the Vermenagna Valley. The southern (French) side encompasses the Roya, Vésubie, and Tinée valleys. The large-scale morphology and drainage pattern of the Maritime Alps are a result of late Alpine tectonics with major fault systems oriented in a NW-SE direction (Ribolini, 2000; Musumeci et al., 2003; Ribolini and Spagnolo, 2008). Bedrock lithologies comprise both crystalline rocks of the Argentera Massif (granites, gneisses, migmatites) and a late Carboniferous to Cenozoic sedimentary cover including limestones, dolomites, quartzites, and sandstones (Malaroda et al., 1970).

Mean annual air temperature at the ARPA Piemonte (https://www.arpa.piemonte.it/) automatic weather station Palanfrè (1625 m a.s.l., see Fig. 2) was 6.7 °C for the period 2002–2022, with July being the hottest (mean of 15.6 °C) and January the coldest (mean of −0.8 °C) month. Precipitation is bimodal with peaks in spring (April/May) and autumn (November). Mean annual precipitation (1971–2008) is around 1300–1500 mm yr^{-1} (Alpine Precipitation Grid Dataset, Isotta et al., 2014), which is lower than in other parts of the south-western Alps and the northern Apennines (Isotta et al., 2014; Crespi et al., 2018). In the mountains, above 1500 m a.s.l., much of the winter (December–April) precipitation falls as snow and snow accumulation can exceed 0.5 m in those months (ARPA Piemonte).

2.2. Glacial history

The Maritime Alps have been shaped by Pleistocene glaciations, resulting in the widespread presence of glacial landforms such as cirques, parabolic-shaped valleys, polished bedrock, and moraine ridges (see Federici et al., 2003 for a detailed geomorphological map). Surface exposure ages exist for a number of glacial oscillations including the LGM, which was dated for the Stura and the Gesso palaeoglaciers, the two largest valley glaciers on the Italian side of the Maritime Alps (reconstructed surface areas: ca. 399 km^2 and ca. 204 km^2). Both glaciers reached their maximum LGM extent at around 25 to 24 ka, recorded by moraines ridges in the lowermost valley tracts (Fig. 2; Federici et al., 2012; Federici et al., 2017; Ribolini et al., 2022a). In both valleys, a second generation of moraines can be found a few kilometres upstream. These moraines were dated to ca. 19 ka, indicating a later phase of glacier advance or stabilisation at the end of the LGM (Federici et al., 2017). During the Late Glacial period, the Stura and Gesso glaciers receded into the upper reaches of their catchments interspersed with temporary advances such as during the Egesen Stadial (Federici et al., 2008; Spagnolo and Ribolini, 2019). Further retreat followed after the Little Ice Age (Federici and Stefanini, 2001) and presently only small niche glaciers and firn patches remain at altitudes above 3000 m a.s.l., predominantly in shaded, north-facing cirques (Federici and Pappalardo, 2010).

Fewer chronological data exist for the LGM on the French side of the Maritime Alps, partly due to the lack of clear frontal moraines in the Tinée and Vésubie valleys (Rolland et al., 2020). According to Julian (1980), the LGM Vésubie Glacier reached Saint-Martin while the Tinée Glacier extended past the gorge downstream of Isola (see Fig. 2; Bigot-Cormier et al., 2005). No numerical ages constrain the maximum glacier expansion, but the onset of deglaciation after the LGM likely occurred between 22 and 18 ka, as suggested by bedrock exposure ages in the upper Tinée Valley (Darnault et al., 2012; ages recalculated by Rolland et al., 2020).

Smaller LGM glaciers, in the order of 1–10 km^2, existed marginal to the main valley glaciers and also in the lower-elevated Vermenagna and Roya valleys, where LGM glaciers remained confined to the upper parts of their catchments (cf. Julian, 1980). The first surface exposure ages for a landform related to these marginal glaciers (Bergemolo moraine, Stura catchment) were recently published by Ribolini et al. (2022a). They point to a glacial maximum around 22 ka; however, the three reported ages display a relatively large spread, and more data is needed to construct robust chronologies at the regional scale.

3. Methods

3.1. Geomorphological survey

A geomorphological survey, aided by topographic maps, aerial photographs, and LiDAR-based digital elevation models (DEMs, ground resolution of 5 m, acquired 2009–2011), was carried out to identify potential study sites in the French and Italian Maritime Alps. The data were retrieved from the geoportals of the Piemonte Region (https://www.geoportale.piemonte.it/cms/) and the French National Institute of Geographic and Forest Information (IGN, https://geoservices.ign.fr/). Existing geomorphological maps were used to identify glacial deposits and landforms in the Gesso, Stura, and Vermenagna valleys (Spinicci, 1994; Federici et al., 2003). The geological map by Malaroda et al. (1970) was consulted to evaluate which catchments contained quartz-bearing lithologies, suitable for the application of ^{10}Be surface exposure dating. Based on this initial survey, the three field sites of Costa Ganola (Gesso catchment), Caramagne (Roya catchment), and Limonetto (Vermenagna catchment) were chosen for a more detailed investigation (see Fig. 2). These sites are characterised by the presence of well-preserved moraine ridges, marginal to the larger LGM glacier systems. Field work at the sites was carried out in October 2021 both to obtain ground control for the geomorphological survey and to collect samples for surface exposure dating.

3.2. Surface exposure dating

A total of 15 samples were collected from erratic boulders located on lateral and frontal moraine ridges at all three sites for ^{10}Be surface exposure dating. The boulders were selected according to a range of criteria, most importantly their size (protruding at least 1 m from the ground) and a central and stable position on the moraine crestline (Ivy-Ochs and Kober, 2008). The sampling was restricted to lithologies that contained macroscopic quartz grains in sufficient quantity, which included both migmatites and quartzites (Malaroda et al., 1970). Flat boulder surfaces without evidence of spalling or anthropogenic reworking were chosen for sampling and depressions were avoided to preclude extensive snow cover. In several instances, the presence of quartz veins protruding from the surrounding rock demonstrated that the surfaces have been subject to prolonged periods of weathering. The material was collected from the boulder surfaces either with an angle grinder or manually using a hammer and chisel. Details on the sampled boulders are listed in Table 1.

The rock samples were crushed and dry-sieved to a grain size of <800 μm using a mechanical jaw crusher (Retsch BB 50) at the Department of Geosciences, University of Padua. Subsequently, they underwent chemical treatment at the Laboratory of Ion Beam Physics, ETH Zurich, according to standardised methods (see Kohl and Nishiizumi, 1992; Ivy-Ochs, 1996). This included selective dissolution of the material in hydrochloric acid (HCl) and several times in weak (4%) hydrofluoric acid (HF) to isolate quartz grains from the mineral

assemblage. For each sample, approximately 15–20 g of purified quartz was then dissolved in concentrated (48%) HF along with 250 μg of a ^{9}Be-carrier. The dissolved samples were passed through exchange resins to remove unwanted ions and Be was isolated via pH-selective precipitation (Kronig et al., 2018).

^{10}Be concentrations were measured with accelerator mass spectrometry (AMS) in the 0.3 MV MILEA system at the Laboratory of Ion Beam Physics, ETH Zurich (for details see Christl et al., 2013). The measurements were performed against the in-house standard S2007N (calibrated against the 07KNSTD, Nishiizumi et al., 2007) and recalculated with a blank correction of (2.98 ± 1.24)*10^{-15}. Exposure ages were then computed with the CRONUS-Earth Calculator (Balco et al., 2008) using the Northeastern North America (NENA) calibration dataset with a constant ^{10}Be production rate of 3.87 ± 0.19 atoms g^{-1} a^{-1} (Balco et al., 2009), a rock density of 2.7 g cm^{-3}, and the scaling scheme for spallation of Lal (1991) and Stone (2000). All ages are reported with 1σ errors, including both internal uncertainties (related to AMS measurements only) and external uncertainties in brackets (also considering uncertainties in the nuclide production rate, Balco et al., 2008).

The exposure ages were corrected assuming a postglacial surface erosion rate of 1 mm ka^{-1}. This rate was adapted in several previous studies in the region (e.g., Baroni et al., 2018; Ivy-Ochs et al., 2018; Braakhekke et al., 2020; Kamleitner et al., 2022) and represents a maximum value for crystalline rocks (André, 2002). The erosion correction increased ages by 1.1–2.5%, which is, except for one boulder (AMLM-4), lower than the respective internal 1σ errors. Additionally, a snow cover correction (following Kronig et al., 2018) was tested using 2002–2022 snow cover data from the Diga del Chiotas automatic weather station (ARPA Piemonte, https://www.arpa.piemonte.it/). This significantly increased exposure ages by ca. 10%. However, in the following, exposure ages will be reported without snow cover correction, because (a) there is no reliable estimate for snow cover evolution during the Holocene and Late Pleistocene, and (b) true snow cover on boulder surfaces was likely much lower than on the ground due to wind-sweeping effects (Ye et al., 2023). No statistical means were calculated for the dated landforms, as distributions of exposure ages tend to be skewed towards younger ages due to various post-depositional processes (Putkonen and Swanson, 2003; Akçar et al., 2011; Heyman et al., 2011). Instead, if not otherwise specified, the oldest age(s) are considered to represent the true age of moraine formation most accurately, especially if they come from large boulders in stable positions. Previously published exposure ages were recalculated according to the methodology described above.

3.3. Reconstructing palaeoglacier 3D-geometries and ELAs

Palaeoglacier 3D-geometries were reconstructed in a geographical information system (*Esri ArcMap v.10.8*) using the GLARE toolbox (Pellitero et al., 2016). This toolbox generates ice thickness points along user-defined flowlines by applying the standard flow law of ice that assumes perfectly plastic ice rheology (Nye, 1952; Schilling and Hollin, 1981; Benn and Hulton, 2010). The flowlines were manually digitised following the course of the valleys, extending from frontal moraines or the lowermost outcrop of glacial diamict up into the cirque headwalls. In the Limonetto catchment, flowlines were also digitised into smaller tributary valleys. The toolbox was initially run with a basal shear stress of 100 kPa in combination with an F-factor correction in areas where glaciers were topographically constrained. The F-factor is a function of the glacier's cross-sectional geometry and accounts for lateral resistance to ice flow from the valley walls (Nye, 1965; Benn and Hulton, 2010). Basal shear stress values were then partially adjusted to match the ice thickness to the geomorphological evidence (i.e., lateral moraine ridges). A kriging interpolation was used to generate ice surface raster files from the thickness points.

ELAs were calculated from the reconstructed ice surfaces using a separate toolbox (Pellitero et al., 2015). Both the Area-Altitude Balance Ratio (AABR, Furbish and Andrews, 1984; Osmaston, 2005; Rea, 2009) and the Accumulation Area Ratio (AAR) methods were applied. An AABR-value of 1.56 and an AAR-value of 0.58 were chosen (Oien et al., 2022). Additionally, glacier volumes and ice thicknesses were estimated by subtracting the present-day DEM from the reconstructed glacier surface raster files.

3.4. Solar radiation modelling

Glacier mass balances and ELAs are controlled by temperature and precipitation (Ohmura et al., 1992; Ohmura and Boettcher, 2018), but can be modulated by local factors, most importantly the catchment topography that governs how the glacier surface is protected from solar radiation (e.g., Coleman et al., 2009; Mills et al., 2012; Chandler and Lukas, 2017). To quantify the effects of such topographic shading, received solar radiation was modelled for the three study sites using the "Area Solar Radiation" tool in *Esri ArcGIS Pro v.3.1* with a uniform overcast sky. Two different settings are distinguished: In the first setting, radiation is modelled across the entire present-day catchments, including areas of potential snow accumulation outside the limits of the reconstructed glaciers (i.e. simulating conditions in which glaciation would start). For the second setting, the tool was run with the reconstructed ice surfaces as input, simulating radiation in an "LGM setting" when valleys were occupied by ice. Radiation values were calculated on a daily basis for the summer months June, July, and August when most melt occurs. For each catchment/glacier surface a mean radiation value was calculated to facilitate a comparison between the three sites. It should be noted that modern values for radiation were used i.e., not those at the LGM, but this is assumed to have a negligible effect for the purposes of this research.

4. Results

4.1. Geomorphology and surface exposure ages

4.1.1. Costa Ganola

The Costa Ganola site is located ca. 3 km south of Entracque, at the confluence of the Gesso della Barra and the Bousset rivers (Fig. 3A). The catchment comprises a single north-facing cirque (cirque floor altitude ca. 1870 m a.s.l.) with a steep headwall that reaches its highest point at a northern spur of Monte Aiera (ca. 2450 m a.s.l.). The former extent of the glacier occupying the Costa Ganola catchment is marked by a pair of lateral to frontal moraine ridges that reach a minimum elevation of 1100 m a.s.l. (Fig. 3B; Fig. 3C). These moraines attain a height of ca. 60 m and a crest length of over 700 m (right moraine) and 400 m (left moraine), respectively. Erratic boulders occur frequently on top of their well-defined crestlines (Fig. 3D; Fig. 3E). Just outside the limits of the Costa Ganola catchment, there is another prominent moraine ridge, the Serrera dei Castagni moraine, that has a crest length of over 2 km. This moraine can be interpreted as a left lateral moraine deposited by a tributary of the Gesso Glacier in the Bousset Valley.

Seven samples were taken from boulders at Costa Ganola for surface exposure dating. Five of the samples were processed for age determination (Table 1), all of which are located in the upper part of the right lateral moraine. Three ages (AMCG-4, -6, and -7) are in very good agreement with each other at 19.4 ± 0.6 (1.1) ka, 19.1 ± 0.6 (1.1) ka, and 19.2 ± 0.5 (1.1) ka, respectively. Also the age of AMCG-3 (18.2 ± 0.5 (1.0) ka) is within the uncertainty range of these results, while AMCG-5 (17.1 ± 0.5 (1.0) ka) yielded a slightly younger age. No suitable boulders were found for dating the formation of the Serrera dei Castagni moraine.

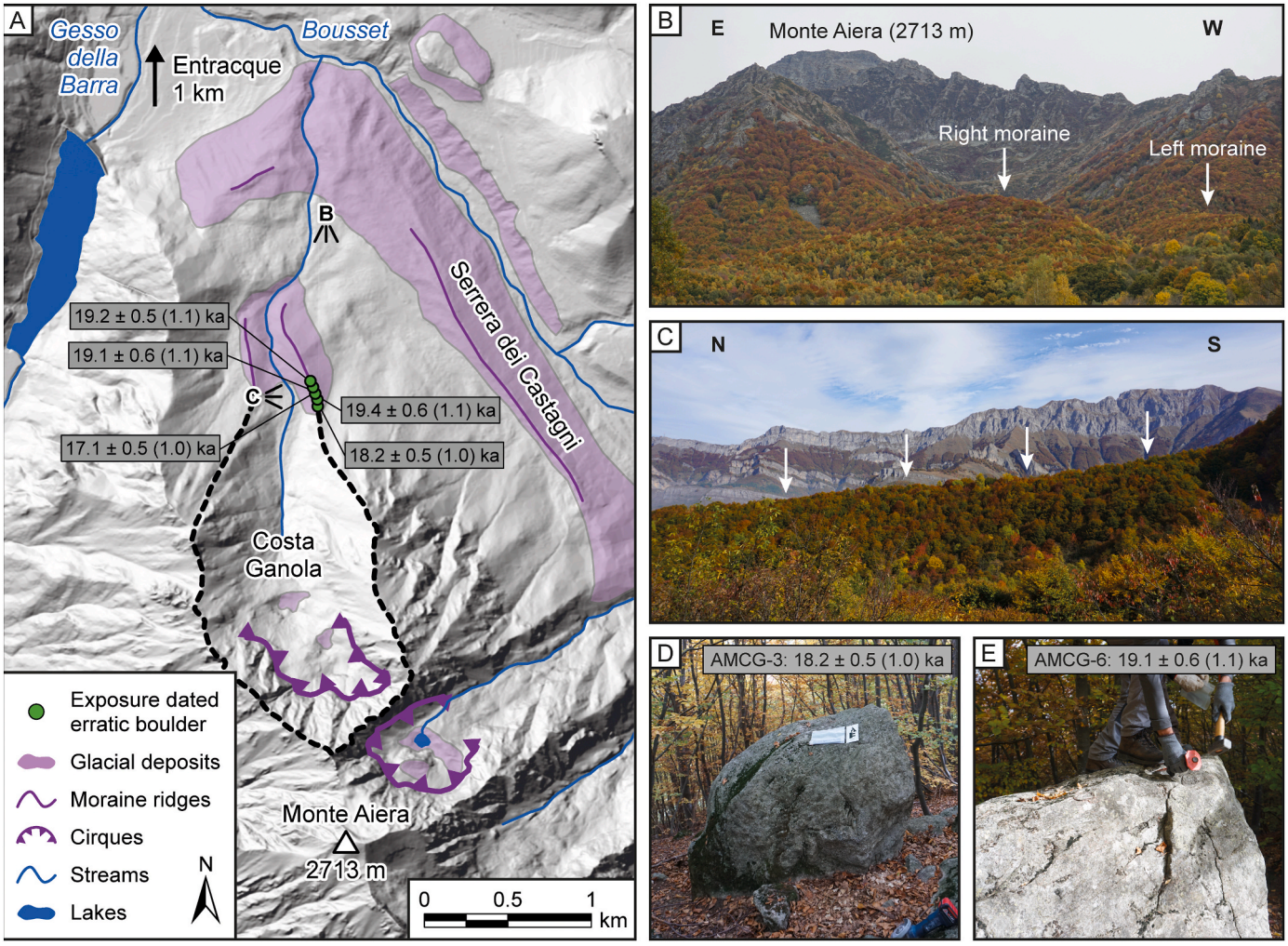

Fig. 3. A. Geomorphological sketch map of the Costa Ganola site, including the results of surface exposure dating from erratic boulders. The outline of the Costa Ganola catchment is marked by a dashed black line. Locations of photos B, and C are indicated in the map. Underlying elevation data: RIPRESA AEREA ICE 2009–2011 - DTM 5 (https://www.geoportale.piemonte.it/cms/). **B.** View towards Monte Aiera and the Costa Ganola cirque. The frontal moraines can be seen in the foreground and are marked by white arrows. **C.** The crestline of the right moraine ridge, marked by white arrows. **D.** Boulder AMCG-3, sampled for surface exposure dating. **E.** Sampling boulder AMCG-6 manually using hammer and chisel.

4.1.2. Caramagne

The Caramagne Valley (French: *Vallon de Caramagne*) is situated on the southern (French) side of the main divide of the Maritime Alps (Fig. 4A). The headwall of the valley is framed by Cima del Sabbione (2610 m a.s.l.) and Rocca dell'Abisso (2755 m a.s.l.), the latter peak separating the catchment from the Gesso Valley to the north-west and the Vermenagna Valley to the north-east. A low-elevated saddle (Baisse de Peyrefique) divides the Caramagne Valley from the Casterine-Valmasque Valley to its south. The upper part of the Caramagne catchment is wide and has a southern to south-eastern aspect. In its lower reaches, the valley becomes increasingly narrow, stretching down to an elevation of ca. 1100 m a.s.l. A prominent lateral moraine with a crest length of ca. 2.7 km can be found on the left side of the lower Caramagne Valley. The crestline of this moraine is rather wide and smooth and is, in parts, composed of two single crests running in parallel (Fig. 4B). No equivalent lateral moraine is preserved on the right side of the valley.

Four samples were taken from boulders on the left lateral moraine ridge in the Caramagne Valley for surface exposure dating (Fig. 4C; Fig. 4D; Table 1). All of these boulders are from the upper part of the moraine, upstream of where the ridge splits into two separate crests. Two dates (AMCM-1, and -4) are in good agreement with each other at 24.6 ± 0.9 (1.5) ka, and 24.3 ± 0.8 (1.4) ka, respectively. Samples AMCM-2 (19.3 ± 0.6 (1.1) ka) and AMCM-3 (16.7 ± 0.5 (0.9) ka) yielded significantly younger ages.

4.1.3. Limonetto

The Limonetto site (Fig. 5A) is located in the upper sector of the Vermenagna Valley, which is separated from the Caramagne catchment by a crest that extends from Rocca dell'Abisso (2755 m a.s.l.) to the Tenda Pass. The valley has a north-easterly orientation, and its upper parts are carved in bedrock that shows clear signs of ice-moulding, such as roche moutonnées (Fig. 5B). Farther down, two tributary valleys merge with the trunk valley, the Salante Valley to its south-east, and a valley to the west of Monte Ciotto Mien (2378 m a.s.l.). Several moraine ridges can be found in the lower-elevated areas, around the town of Limonetto (Fig. 5C). On the left side of the valley, a lateral moraine ridge extends for ca. 1.5 km, covered by rather small boulders that can be linked to the palaeoglacier accumulation areas carved in high-grade metamorphic and granitoid rocks (Fig. 5D). A second moraine ridge is located further downstream on the right side of the valley. Here, erratic boulders are much larger but some of them appear to have slid or

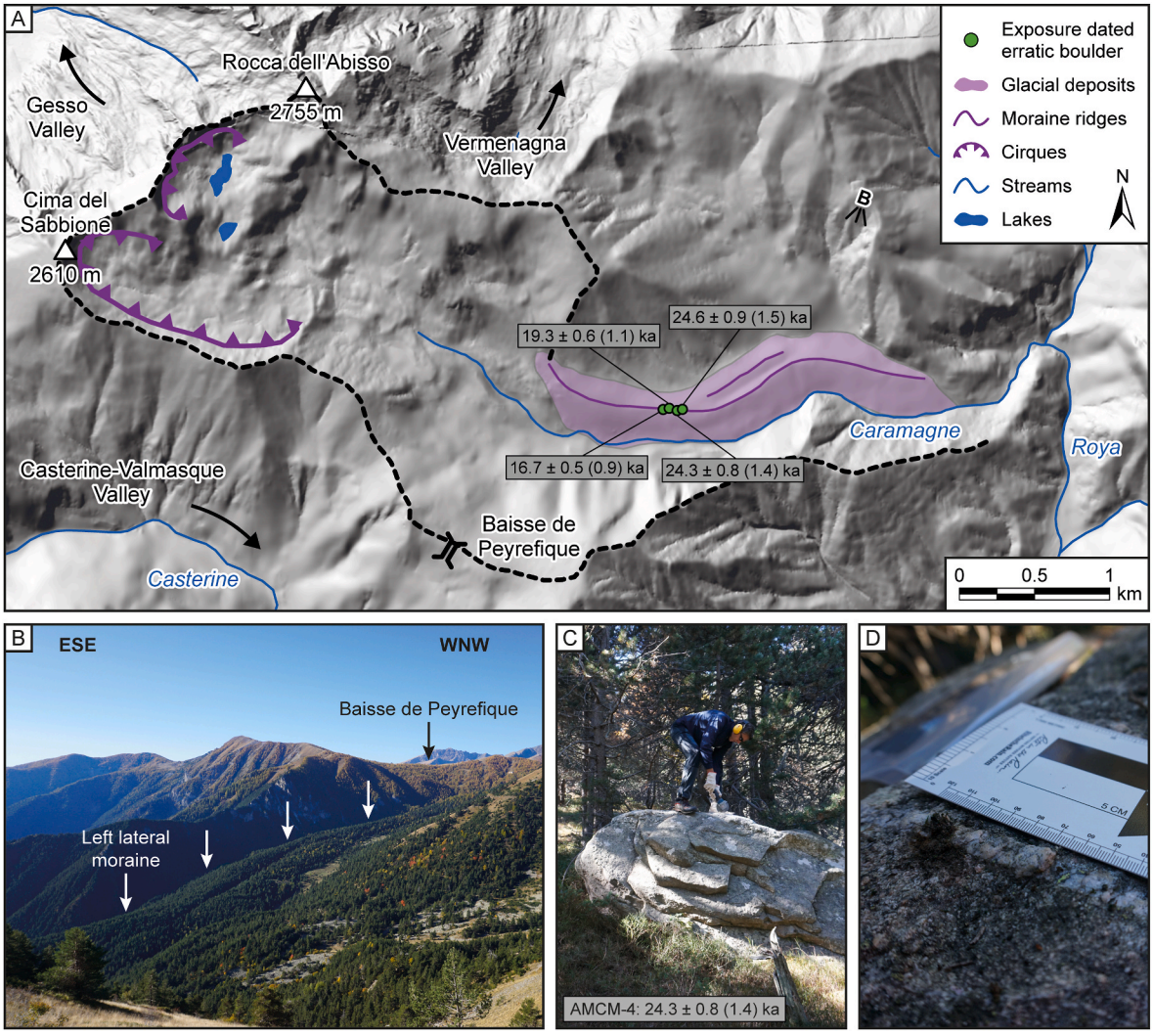

Fig. 4. A. Geomorphological sketch map of the Caramagne Valley, including the results of surface exposure dating from erratic boulders. The outline of the Caramagne catchment is marked by a dashed black line. Location of photo B is indicated in the map. Underlying elevation data: RIPRESA AEREA ICE 2009–2011 - DTM 5 (https://www.geoportale.piemonte.it/cms/) and RGE ALTI DTM (https://geoservices.ign.fr/). **B.** View towards the lateral moraine in the Caramagne Valley (marked by white arrows). In the background, the Baisse de Peyrefique can be seen. **C.** Boulder AMCM-4, sampled with an angle grinder for surface exposure dating. **D.** A protruding quartz vein on boulder AMCM-1 indicates that its surface has been subject to a prolonged period of weathering.

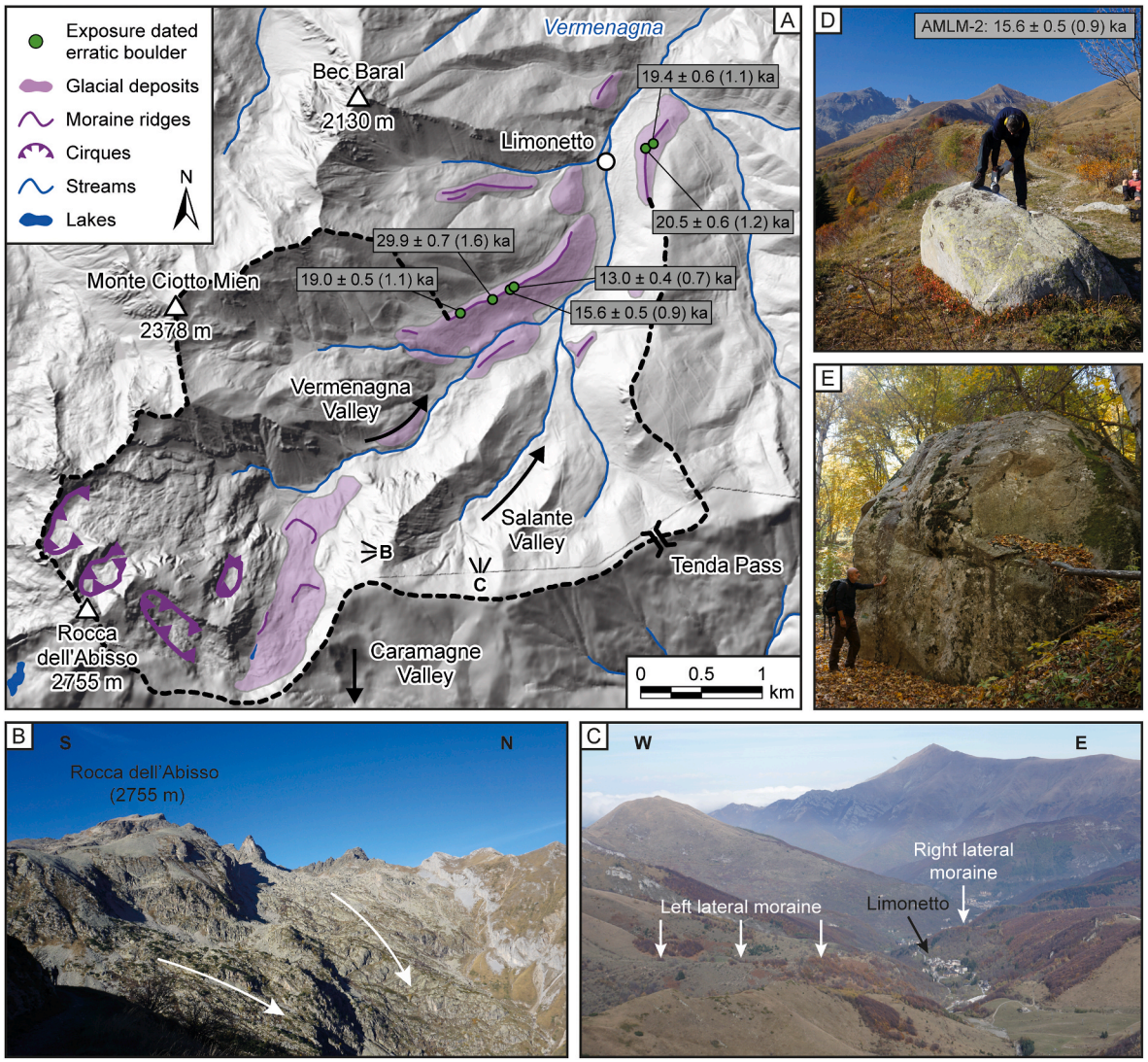

Fig. 5. A. Geomorphological sketch map of the Limonetto site in the upper Vermenagna Valley, including the results of surface exposure dating from erratic boulders. The outline of the upper Vermenagna catchment is marked by a dashed black line. Locations of photos B, and C are indicated in the map. Underlying elevation data: RIPRESA AEREA ICE 2009–2011 - DTM 5 (https://www.geoportale.piemonte.it/cms/) and RGE ALTI DTM (https://geoservices.ign.fr/). **B.** Glacially-moulded bedrock around Rocca dell'Abisso. Former ice-flow direction is indicated by white arrows. **C.** View towards the town of Limonetto and the left and right lateral moraine ridges (marked with white arrows). **D.** Boulder AMLM-2, sampled for surface exposure dating. **E.** A large erratic boulder on the right moraine ridge close to Limonetto. Due to its position on the slope of the moraine, this boulder was not sampled for surface exposure dating.

toppled from the crestline and are now positioned on the slopes of the moraine (Fig. 5E). Downstream of Limonetto, the Vermenagna Valley is affected by anthropogenic reworking and no further glacial landforms or sediments were found.

The ages from the six samples collected from boulders on the Limonetto moraines display a relatively large spread (Table 1). This is especially the case for the left lateral moraine: samples AMLM-1, -2, -3, and -4 yielded ages of 19.0 ± 0.5 (1.1) ka, 15.6 ± 0.5 (0.9) ka, 13.0 ± 0.4 (0.7) ka, and 29.9 ± 0.7 (1.6) ka, respectively. The two samples that were collected from the right moraine show a better agreement at 19.4 ± 0.6 (1.1) ka (AMLM-5) and 20.5 ± 0.6 (1.2) ka (AMLM-6).

4.2. Glacier reconstructions and ELAs

Using the geomorphological evidence presented above, a reconstruction of the 3D-geometries and ELAs for the Costa Ganola, Caramagne, and Limonetto glaciers was carried out. The reconstructed glaciers are shown in Fig. 6 and additional metrics are listed in Table 2. The Costa Ganola cirque hosted the smallest of the three glaciers (Fig. 6A) with a surface area of ca. 0.96 km^2, an estimated volume of ca. 0.03 km^3, and a maximum thickness of 80 m. The ELA of the Costa Ganola Glacier was reconstructed at 1620 m a.s.l. using the AABR-method and at 1610 m a.s.l. using the AAR-method. The Caramagne Glacier (Fig. 6B) was considerably larger both in surface area (ca. 5.0 km^2), volume (ca. 0.26 km^3), and thickness (125 m). The ELA of the Caramagne Glacier was calculated to 1980 m a.s.l. (AABR) and to 2040 m a.s.l. (AAR).

For the reconstruction of the Limonetto Glacier, two different scenarios were considered. In a first scenario (represented in Fig. 6C), the smaller tributary in the Salante Valley merged with the larger trunk glacier. In this case, the reconstructed Limonetto Glacier had a surface area of ca. 9.3 km^2, an estimated volume 0.64 km^3, and a maximum thickness of 220 m. In the second scenario, the Limonetto and Salante glaciers remained disconnected even at their maximum extents. For this case, a surface area of 7.28 km^2 was determined for the Limonetto Glacier. The reconstructed ELAs for both scenarios, however, are remarkably similar with 1790 m a.s.l. assuming a confluence and 1800 m a.s.l. assuming no confluence (both values calculated with an AABR of

Table 1
Details of sampled boulders and results of ^{10}Be surface exposure dating at Costa Ganola, Caramagne, and Limonetto. Exposure ages are reported assuming a surface erosion rate of 1 mm ka^{-1}, without snow cover correction and with internal 1σ errors (external uncertainties in brackets).

Sample ID	Location	Lithology	Boulder size (L x W x H) [m]	Latitude [°N]	Longitude [°E]	Elevation [m a.s.l.]	Sample thickness [cm]	Topographic shielding factor	^{10}Be concentration [*10^5 atoms g^{-1}]	Exposure age (1 mm ka^{-1} erosion) [ka]
AMCG-3	Costa Ganola	Migmatite	2.5 x 2.0 x 1.3	44.2119	7.4079	1365	2.8	0.9732	2.085 ± 0.060	**18.2 ± 0.5 (1.0)**
AMCG-4	Costa Ganola	Migmatite	3.5 x 3.0 x 1.1	44.2121	7.4079	1365	2.5	0.9747	2.223 ± 0.066	**19.4 ± 0.6 (1.1)**
AMCG-5	Costa Ganola	Migmatite	2.5 x 2.0 x 1.1	44.2122	7.4079	1365	2.5	0.9752	1.966 ± 0.059	**17.1 ± 0.5 (1.0)**
AMCG-6	Costa Ganola	Migmatite	4.0 x 3.5 x 1.4	44.2127	7.4077	1360	2.9	0.9794	2.180 ± 0.065	**19.1 ± 0.6 (1.1)**
AMCG-7	Costa Ganola	Migmatite	2.0 x 2.0 x 1.0	44.2132	7.4073	1355	1.7	0.9819	2.214 ± 0.060	**19.2 ± 0.5 (1.1)**
AMCM-1	Caramagne	Quarzite	3.0 x 2.0 x 1.8	44.1249	7.5339	1690	2.5	0.9596	3.515 ± 0.130	**24.6 ± 0.9 (1.5)**
AMCM-2	Caramagne	Quarzite	3.0 x 3.0 x 1.5	44.1249	7.5344	1685	1.8	0.9869	2.844 ± 0.080	**19.3 ± 0.6 (1.1)**
AMCM-3	Caramagne	Quarzite	2.0 x 2.0 x 0.8	44.1248	7.5350	1675	1.6	0.9772	2.428 ± 0.067	**16.7 ± 0.5 (0.9)**
AMCM-4	Caramagne	Quarzite	4.0 x 2.0 x 1.5	44.1249	7.5355	1670	1.5	0.9897	3.542 ± 0.107	**24.3 ± 0.8 (1.4)**
AMLM-1	Limonetto	Quarzite	3.0 x 2.5 x 1.2	44.1661	7.5418	1625	2.0	0.9879	2.692 ± 0.072	**19.0 ± 0.5 (1.1)**
AMLM-2	Limonetto	Quarzite	3.0 x 2.0 x 1.0	44.1671	7.5451	1565	1.2	0.9874	2.133 ± 0.064	**15.6 ± 0.5 (0.9)**
AMLM-3	Limonetto	Quarzite	3.0 x 2.0 x 1.5	44.1679	7.5469	1530	2.0	0.9613	1.680 ± 0.051	**13.0 ± 0.4 (0.7)**
AMLM-4	Limonetto	Quarzite	3.5 x 3.0 x 1.7	44.1681	7.5473	1530	2.2	0.9892	3.892 ± 0.085	**29.9 ± 0.7 (1.6)**
AMLM-5	Limonetto	Quarzite	7.0 x 4.0 x 1.5	44.1785	7.5606	1320	1.6	0.9942	2.205 ± 0.067	**19.4 ± 0.6 (1.1)**
AMLM-6	Limonetto	Quarzite	6.0 x 6.0 x 1.8	44.1789	7.5613	1310	1.9	0.9942	2.302 ± 0.063	**20.5 ± 0.6 (1.2)**

1.56). This demonstrates that the smaller tributaries did not strongly affect the mass balance of the much larger trunk glacier.

4.3. Solar radiation modelling

The results of modelling received solar radiation across the three formerly glaciated catchments are reported in Table 2 and visualised in Fig. 7. Among the three sites, the Costa Ganola catchment receives the lowest surface averaged radiation (413 ± 47 kWh m^{-2}), in line with its northerly aspect (Fig. 7A). The Limonetto catchment (Fig. 7B) receives higher amounts of radiation (465 ± 49 kWh m^{-2}), while the highest mean values were calculated for the south-east facing Caramagne catchment (Figs. 7C and 490 ± 54 kWh m^{-2}). The same patterns can be observed when limiting the radiation modelling to the respective glacier surfaces, with absolute values being slightly higher, due to the generally smoother topographies of the ice surfaces.

5. Discussion

5.1. LGM chronology in the Maritime Alps

The set of 15 new surface exposure ages presented in section 4.1. enables us to strengthen the LGM chronology in the Maritime Alps and to compare the responses of smaller cirque and valley glaciers to those of the larger Gesso and Stura systems (see Fig. 8; ages recalculated from Federici et al., 2012; Ribolini et al., 2022a). In the following, exposure ages will be reported with internal 1σ uncertainties only (for external uncertainties see Table 1).

The earliest evidence for an LGM ice advance in the Maritime Alps comes from the left lateral moraine in the Caramagne Valley (Fig. 8A). This moraine was likely formed between ca. 25 and 24 ka, as indicated by the consistent ages of boulders AMCM-1 (24.6 ± 0.9 ka) and AMCM-4 (24.3 ± 0.8 ka). The date of boulder AMCM-2 (19.3 ± 0.6 ka) possibly indicates a readvance of the Caramagne Glacier slightly before 19 ka, at the end of the LGM. Such a two-phase glacier advance could also be reflected in the prominent morphology of the Caramagne moraine and its two separate crestlines. However, the limited availability of suitable boulders precluded the possibility of sampling the two crests separately and therefore such a two-fold advance remains somewhat speculative from a chronological perspective. The ages from the Caramagne Valley are in close agreement with chronological data from the Stura Valley, where three boulders from the Bedoira moraine yielded exposure ages of 24.3 ± 1.5 ka, 24.5 ± 1.0 ka, and 25.7 ± 1.7 ka (Fig. 8B, Ribolini et al., 2022a; note the higher uncertainties). This is also consistent with data from the Tetti del Bandito moraine in the Gesso Valley (Fig. 8C, two boulders dated 25.0 ± 1.2 ka and 22.4 ± 1.1 ka; Federici et al., 2012) and to a lesser extent from the Bergemolo moraine, related to a marginal glacier in the Stura catchment (Fig. 8D, one boulder dated to 23.0 ± 1.6 ka; Ribolini et al., 2022a).

Stronger evidence for a second LGM glacier advance, just before 19 ka, comes from Costa Ganola (Fig. 8E), as indicated by the close match between the exposure ages from boulders AMCG-4 (19.4 ± 0.6 ka), AMCG-6 (19.2 ± 0.5 ka), and AMCG-7 (19.1 ± 0.6 ka). The younger dates of boulders AMCG-3 (18.2 ± 0.5 ka) and AMCG-5 (17.1 ± 1.0 ka) are probably the result of incomplete exposure due to post-depositional exhumation or toppling, as commonly observed in exposure age datasets (Heyman et al., 2011). No data supporting an earlier advance of the Costa Ganola Glacier around 24 ka was found. However, it is possible that during such an earlier stage the Costa Ganola Glacier was more extensive and merged with the tributary of the Gesso Glacier in the Bousset Valley (this interpretation was adopted in Federici et al., 2012).

The exposure ages from boulders on the left lateral moraine at Limonetto (Fig. 8F) display a large spread. Many boulders on the crest of the moraine are rather small, which enhances the potential for post-depositional exhumation. Indeed, the two smallest boulders (AMLM-2, and -3) also yielded the youngest ages (15.6 ± 0.5 ka and 13.0 ± 0.4 ka, respectively). The relatively old date of AMLM-4 (29.9 ± 0.7 ka), on the other hand, may be the result of inheritance, as the moraine is located close to a steep rock wall. The exposure ages of the two boulders from the right lateral moraine at Limonetto, AMLM-5 (19.4 ± 0.6 ka) and AMLM-6 (20.5 ± 0.6 ka), show better agreement. From a morphological point of view, however, the two moraines can be seen as an expression of the same glacier advance as their elevations match well with the surface profile of the reconstructed Limonetto Glacier (see section 4.2.). In total, three of the six ages from Limonetto fall into the period between 20.5 and 19 ka which therefore appears the best estimate for the advance of the glacier. These dates also largely correspond to the advance of the Costa Ganola Glacier and the potential re-advance of the Caramagne Glacier mentioned earlier.

The formation of moraines at Costa Ganola and Limonetto, between 19 and 20.5 ka can chronologically be linked to recessional moraines in the Stura and Gesso valleys. In the Stura Valley, two boulders from the Festiona moraine yielded exposure ages of 20.3 ± 0.7 ka and 18.8 ± 0.7 ka (Fig. 8G, Ribolini et al., 2022a), and in the Gesso Valley, the two oldest ages from the Ponte Murato moraine are 20.5 ± 0.9 ka and 19.4 ± 0.8 ka (Fig. 8H, Federici et al., 2012). This latter frontal moraine can morphologically be linked to the Serrera di Castagni lateral moraine (see Fig. 3), suggesting that its formation was likely contemporaneous with the moraines at Costa Ganola.

The LGM advances of small and large valley glaciers throughout the Maritime Alps appear synchronous within the uncertainty of the exposure ages. This suggests that both the larger Gesso and Stura and the

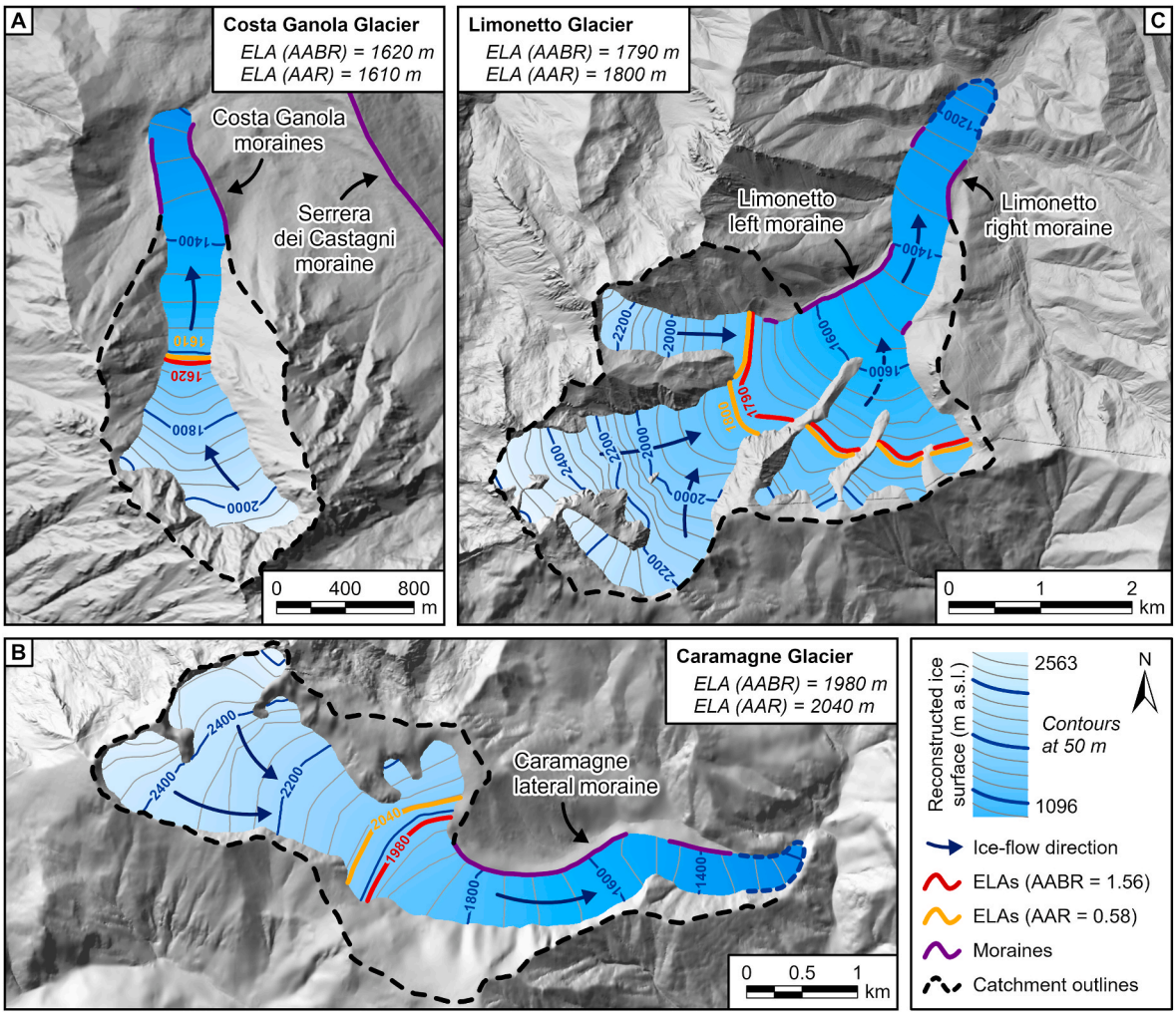

Fig. 6. Reconstructed ice surfaces and ELAs for **(A)** the Costa Ganola Glacier, **(B)** the Caramagne Glacier, and **(C)** the Limonetto Glacier during the LGM. For the Limonetto Glacier, a confluence with the tributary in the Salante Valley is assumed. The frontal positions of the Caramagne and Limonetto glaciers are approximate, as no frontal moraines were preserved (uncertainties in the reconstruction are indicated by dashed blue lines). Underlying elevation data: RIPRESA AEREA ICE 2009–2011 - DTM 5 (https://www.geoportale.piemonte.it/cms/) and RGE ALTI DTM (https://geoservices.ign.fr/).

Table 2
Properties and ELAs of the reconstructed Costa Ganola, Caramagne, and Limonetto glaciers during their LGM maximum extent. The data for the Gesso and Stura glaciers were calculated from Federici et al. (2012); Ribolini et al. (2022a).

Glacier name	Exposition	Minimum elevation [m a.s.l.]	Maximum Elevation [m a.s.l.]	Surface Area [km^2]	Ice Volume [km^3]	Maximum Thickness [m]	Flowline length [km]	**ELA (AABR 1.56) [m a.s.l.]**	ELA (AAR 0.58) [m a.s.l.]	**Received solar radiation (JJA)**	
										Catchment [kWh m^{-2}]	Ice surface [kWh m^{-2}]
Costa Ganola	North	1175	2100	1.0	0.03	80	2.7	**1620**	1610	413 ± 47	443 ± 23
Caramagne	South-East	1145	2620	5.0	0.26	125	6.8	**1980**	2040	490 ± 54	522 ± 28
Limonetto	North-East	1090	2610	9.3	0.64	220	8.4	**1790**	1800	465 ± 49	488 ± 24
Gesso	North-East	730	3125	204	29.2	525	ca. 27	**1850**	1840	443 ± 65	486 ± 39
Stura	East	630	2890	309	53.5	620	ca. 51	**1800**	1860	465 ± 54	501 ± 32

smaller Costa Ganola, Caramagne, and Limonetto glaciers essentially responded synchronously (within methodological uncertainties) to climatic forcing during the LGM and the early deglaciation. Despite this chronological similarity, there is a difference in the way these advances are preserved in the geomorphological record. In the Stura and Gesso Valleys, the late LGM recessional moraines are located several kilometres upstream of the respective LGM maximum. The Gesso Glacier terminus, for example, retreated around 5 km from its maximum position to its late LGM recessional moraine and the front of the Stura Glacier receded by 7 km during the same time interval. This change was accomplished by only a minor shift in ELA (Federici et al., 2012, 2017; Ribolini et al., 2022b). This can be explained by the fact that both the Stura and the Gesso glaciers were characterised by long and gently sloping ablation areas. A minor change in climate (and hence ELA) therefore resulted in a relatively large change in their frontal positions. In contrast, there is no morphological expression of the same minor shift in climate for the studied smaller glaciers, where only one moraine system is recorded at each site.

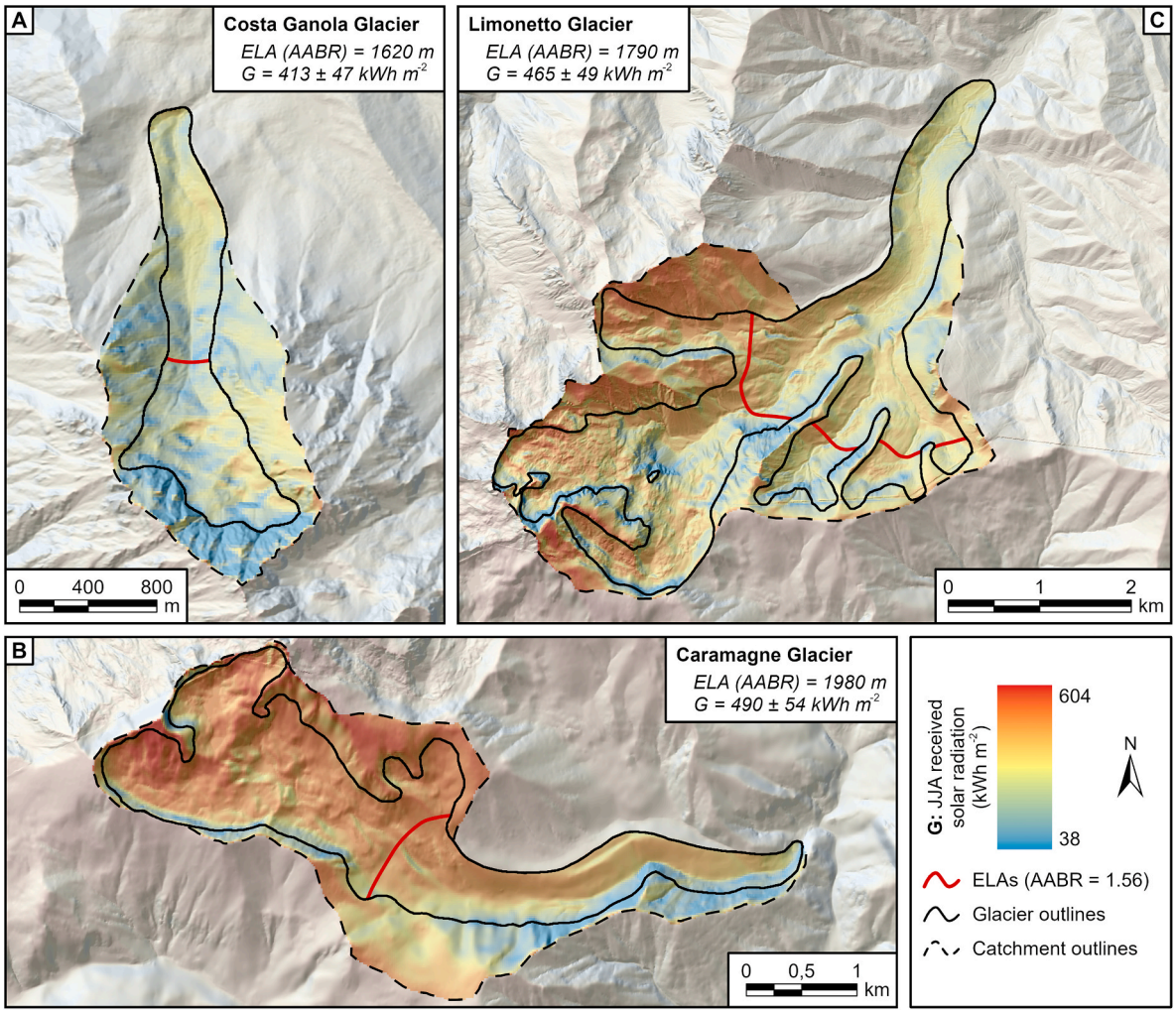

Fig. 7. Modelled received solar radiation (G) over the summer months June, July, and August across (A) the Costa Ganola, (B) the Caramagne, and (C) the Limonetto catchments. The red line represents the LGM ELA, calculated for the respective glacier surfaces with an AABR of 1.56.

This observation suggests an important influence of topography and glacier hypsometry on how glacier advances, even under the same climatic forcing, are transferred into the morphological record. Larger glaciers may preserve climatic fluctuations as series of recessional moraines, each of which can be dated to obtain chronological control on glacier and climate change. Smaller glaciers, on the other hand, likely stay at, or advance several times to, a similar frontal position if changes in climate (and hence ELA) are minor. Frontal and lateral moraines related to smaller glacier therefore often represent multiple glacier advances (cf., Lukas et al., 2012) and consequently dating these landforms may reveal only the last of potentially several advances.

5.2. Comparisons to LGM chronologies from the south-western Alps

The chronological pattern described in section 5.1. is not unique to the Maritime Alps but can be observed throughout the south-western Alps, where similar surface exposure ages have been reported from most of the major LGM morainic amphitheatres (Fig. 9). The maximum extent of the Ticino-Toce glacier was dated between 25.0 ± 0.9 ka and 19.9 ± 0.7 ka in the Verbano amphitheatre, with a short-lived readvance occurring at 19.7 ± 1.1 ka (Kamleitner et al., 2022). The Orta glacier reached its LGM maximum between 26.5 and 23 ka, with a recessional phase recorded around 19 ± 1 ka (Braakhekke et al., 2020). In the Rivoli-Avigliana end-moraine system, the LGM maximum and recessional phase of the Susa Glacier occurred at 24.0 ± 1.5 and 19.6 ± 0.9 ka, respectively (Ivy-Ochs et al., 2018). Luminescence datings from the Lyon lobe, on the western (French) side of the Alps, suggested that this glacier had its maximum extent already earlier during MIS 3 or 4 (Gribenski et al., 2021). However, new surface exposure ages were recently reported by Roattino et al. (2022), constraining the maximum LGM extent between 24 and 21 ka and a withdrawal phase at ca. 19 ka, in line with its counterparts to the east.

To summarise, there seems to be a synchronous response of glaciers in the south-western Alps to LGM climatic changes, despite the large differences in the sizes of their catchments, ranging from several thousand km^2 (e.g., Ticino-Toce Glacier, Kamleitner et al., 2022) down to less than 1 km^2 (Costa Ganola Glacier). The assumption that smaller glaciers will have responded faster to LGM climatic forcing remains therefore valid only within the uncertainties of the dating method of ca. ± 1 ka.

5.3. ELAs and local topoclimate

Reconstructing ELAs from palaeoglaciers can provide important information on the climate of the past and has been recently used to quantify LGM-precipitation in the Alpine region (Baroni et al., 2018; Ribolini et al., 2022a; Rettig et al., 2023). For such palaeoclimatic inferences, however, it is crucial to establish that reconstructed glacier ELAs are climatically controlled. In this context it is notable that the ELA values of the three glaciers in the Maritime Alps show a large

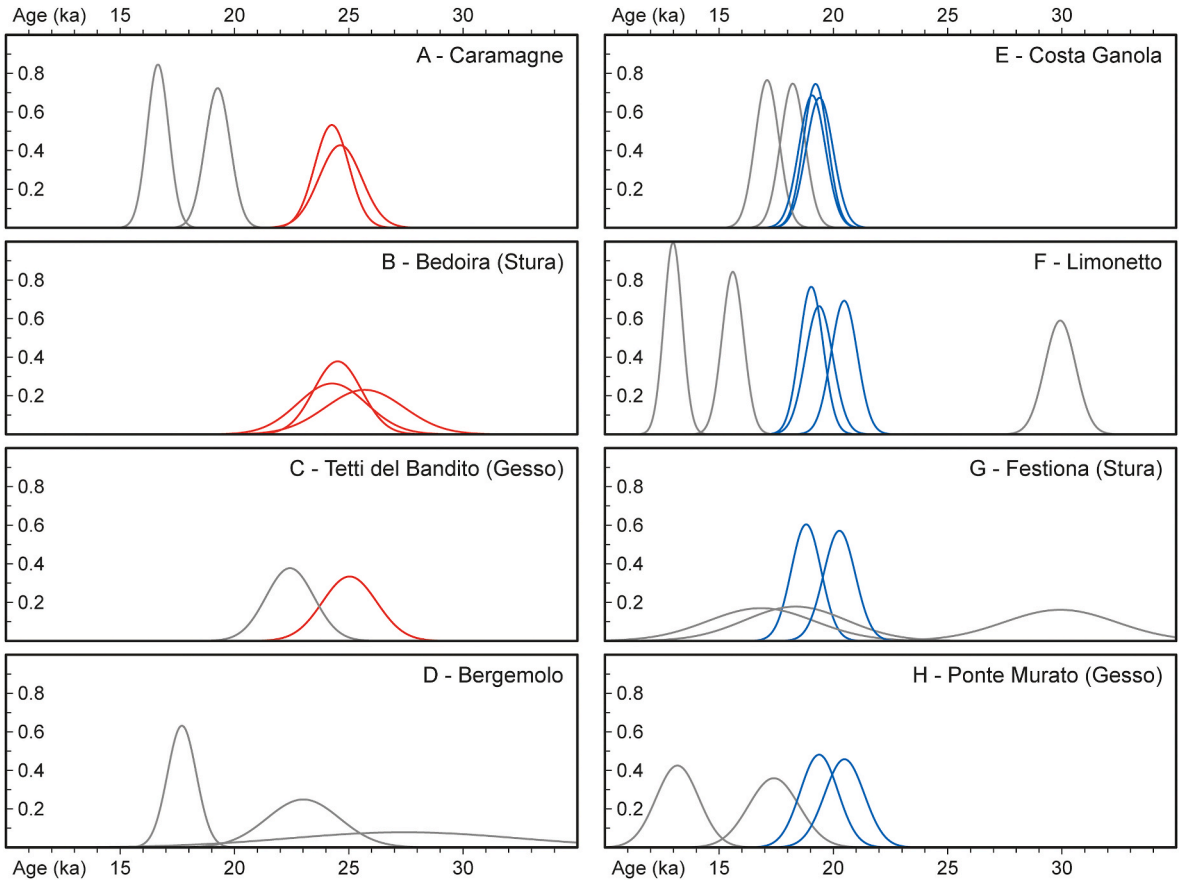

Fig. 8. An overview of LGM surface exposure ages from the Maritime Alps, including both the new data reported in this study and those from the Gesso (recalculated from Federici et al., 2012), Stura, and Bergemolo (recalculated from Ribolini et al., 2022a) glaciers. Exposure ages are represented as probability curves with internal 1σ uncertainties. Panels A–D: Ages related to the early LGM (ca. 25 to 24 ka) maximum extent (marked in red). Panels E–H: Ages related to a late LGM (ca. 20.5 to 19 ka) recessional phase (marked in blue).

discrepancy. The difference (ΔELA = 360 m) between the ELAs of the Costa Ganola Glacier (1620 m a.s.l.) and the Caramagne Glacier (1980 m a.s.l.), only a few kilometres apart, is especially striking. It is at the maximum end of what is observed for modern glaciers (cf. Evans and Cox, 2005) and suggests that the mass balances of these glaciers were not only affected by a regionally homogenous climatic forcing but also by local topoclimatic factors, related to the specific geometry and aspect of their catchments (e.g., Benn and Ballantyne, 2005; Coleman et al., 2009; Chandler and Lukas, 2017). The low ELA of the Costa Ganola Glacier is in line with its north-facing catchment and steep cirque headwall that partly shielded it from incoming solar radiation. Averaged across the catchment, received solar radiation is by far the lowest among the three glaciers in this study. This is in stark contrast to the Caramagne Glacier with its wide, south-east facing accumulation area that received substantially higher amounts of radiation across its catchment.

The ELA of the Limonetto Glacier (1790 m a.s.l.) corresponds with the ELAs of the larger Gesso (1850 m a.s.l.; recalculated from Federici et al., 2012) and Stura (1800 m a.s.l.; recalculated from Ribolini et al., 2022a) glaciers and also the Bergemolo glacier (1821 m a.s.l., Ribolini et al., 2022a). The modelled received ablation season radiation for the Limonetto (465 ± 49 kWh m^{-2}), Gesso (443 ± 65 kWh m^{-2}), and Stura (465 ± 54 kWh m^{-2}) glaciers are also very similar, suggesting that solar radiation may indeed explain the ELA differences across the region. We therefore consider an ELA of around 1800 m a.s.l. to be most representative for the regional climate in the north-eastern part of the Maritime Alps during the LGM and will refer to this value in the following palaeoclimatic considerations (section 5.4.).

Our observations highlight the importance of considering the effects of local topoclimatic factors that may substantially decouple the glacier ELA from the climatic conditions. Ideally, palaeoclimatic interpretations should therefore be based on ELA reconstructions from multiple sites with varying catchment geometries and aspects so that the influence of such topoclimatic factors can be correctly assessed. We propose that modelling received solar radiation using the "Area Solar Radiation" tool can be a quick and easy way to get a first order estimate on one such potential bias, which then should be further explored in the light of the individual sites. Other factors such as snowblow or avalanching (Mitchell, 1996; Benn and Ballantyne, 2005; Coleman et al., 2009; Mills et al., 2012; Kłapyta et al., 2022), for example, were not considered here, mainly due to the difficulty of quantifying such effects. However, these may have been especially significant for the Costa Ganola Glacier that occupied a narrow, north-facing cirque that likely saw substantial avalanche input from its steep headwalls, adding a further explanation to its particularly low ELA. A hypothetical remodelling of the ELA including these headwalls resulted in an ELA of 1760 m a.s.l., which is much closer to the ELA of 1800 m a.s.l. that was considered representative for the regional paleoclimate.

5.4. *Regional palaeoclimate*

The LGM regional glacier ELA for the Maritime Alps of 1800 m a.s.l. is much higher than that of other sites around the Gulf of Genoa (Fig. 9). In the northern Apennines, LGM ELAs range from ca. 1200 m a.s.l. for north-facing glaciers to ca. 1620 m a.s.l. for glaciers with a southern

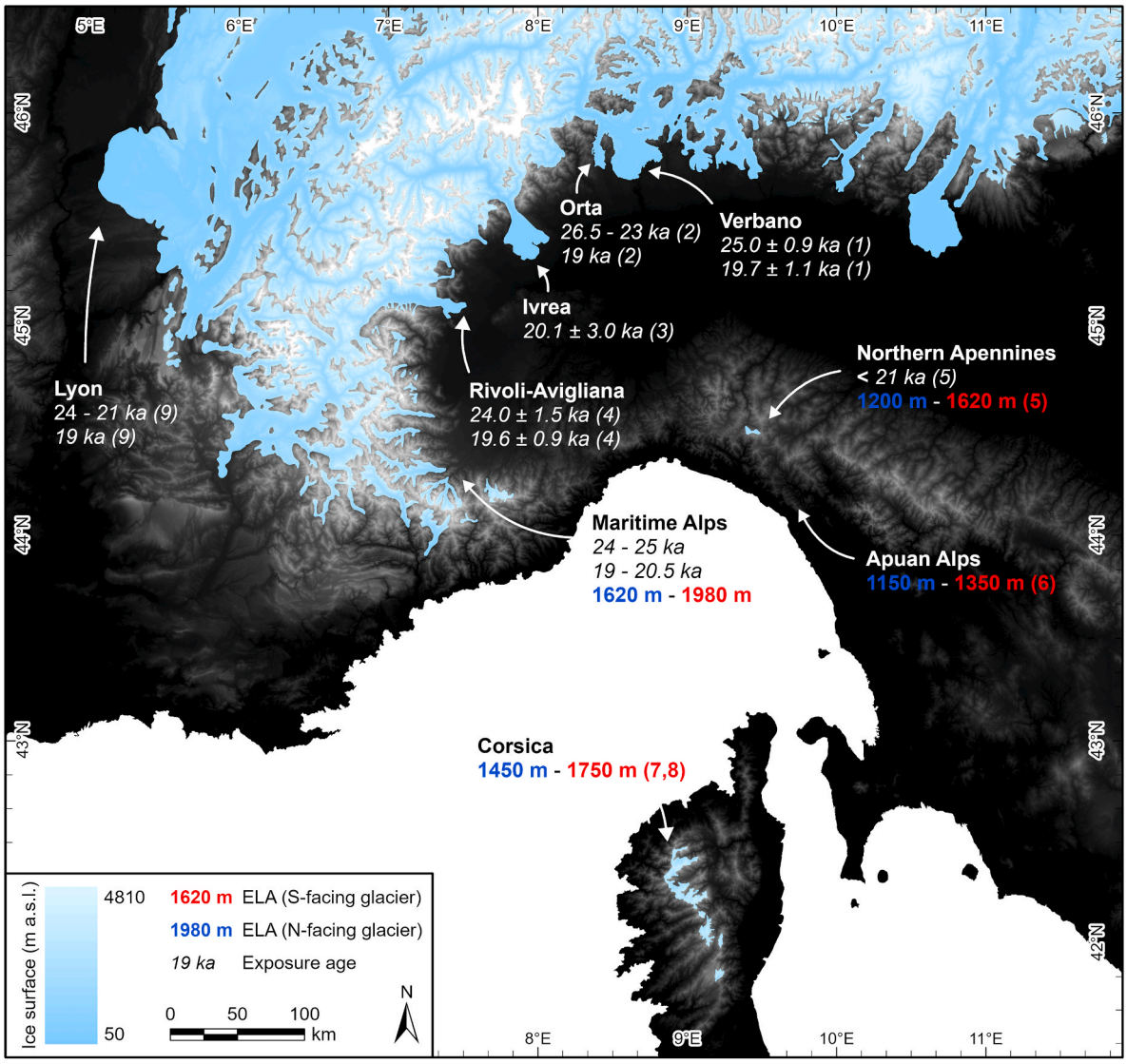

Fig. 9. The Maritime Alps in the framework of the LGM in the western part of the Alps, including previously published exposure ages and ELA estimates. The LGM glacier network was modified from Ehlers and Gibbard (2004). The LGM coastline of the Mediterranean Sea represents a sea level lowering of 120 m (bathymetric data: EMODnet Digital Bathymetry, https://data.europa.eu/data/datasets/emodnet_bathymetry). Surface exposure ages and ELAs taken from (1) Kamleitner et al. (2022), (2) Braakhekke et al. (2020), (3) Gianotti et al. (2015), (4) Ivy-Ochs et al. (2018), (5) Baroni et al. (2018), (6) Baroni et al. (2015), (7) Kuhlemann et al. (2005), and (8) Kuhlemann et al. (2008). The ages in the Maritime Alps represent a synthesis of data from this study and from Federici et al. (2012, 2017) and Ribolini et al. (2022a).

aspect (Giraudi, 2017; Baroni et al., 2018). In the Apuan Alps, ELAs of north-facing glaciers were as low as 1150 m a.s.l. (Baroni et al., 2015; Ribolini et al., 2022b), representing an ELA lowering of about 450 m compared to the Costa Ganola Glacier. In the Corsican mountains, LGM ELAs between ca. 1450 m a.s.l. and 1750 m a.s.l. were reconstructed using an AAR of 0.6, with the higher ELAs related to a more continental climate in the interior parts of the island (Kuhlemann et al., 2005, 2008). Despite the different methods used in these studies, the results also point to significantly lower ELAs as compared to the Maritime Alps.

The relatively high ELA in the Maritime Alps indicates a less humid and/or warmer climate during the LGM. However, given the similar latitude of the sites, large LGM temperature differences seem unlikely. An ELA lowering of 450 m would require temperatures in the Apuan Alps to be ca. 3 °C lower than in the Maritime Alps (assuming a temperature lapse rate of 0.0065 °C m^{-1}). This does not match model-based palaeotemperature reconstructions for the LGM (cf. Del Gobbo et al., 2022). Instead, if a homogenous LGM temperature distribution is assumed, the ELA lowering implies higher rates of precipitation in the Apennines and Apuan Alps. This matches modern climatic patterns in the region, where mean annual precipitation in the Apennines and Apuan Alps is ca. 500 mm yr^{-1} higher than in the Maritime Alps (Isotta et al., 2014; Fratianni and Acquaotta, 2017).

Both palaeoclimate models and proxy data suggest that during the LGM there was an increased moisture supply from the Mediterranean Sea, following a southward shift of the Polar Frontal Jet Stream (Florineth and Schlüchter, 2000; Luetscher et al., 2015; Spötl et al., 2021; Del Gobbo et al., 2022). This was presumably also coupled to increased cyclogenesis in the Gulf of Genoa, transporting humid air masses and enhancing precipitation in the southern Alps and the northern Apennines (Kuhlemann et al., 2008). The north-eastern part of the Maritime Alps, situated in the rain shadow of southern and south-western winds, received significantly less amounts of this southerly-derived precipitation, explaining the generally higher ELAs in this region.

6. Conclusions

In this study, we combined geomorphological mapping with surface exposure dating and numerical glacier reconstructions to gain new insights into the chronology and Equilibrium Line Altitudes of small Last Glacial Maximum (LGM) mountain glaciers in the Maritime Alps (south-western European Alps). A specific focus was to explore potential differences in the responses of smaller and larger Alpine glaciers to LGM climatic changes. The main findings of the study are as follows.

- Surface exposure dating of 15 new erratic boulders indicates a two-fold LGM advance throughout the Maritime Alps. Moraines at one site were formed at 25 to 24 ka while at two other sites a late LGM advance at 20.5 to 19 ka is recognised. This is consistent with ages reported from larger outlet lobes along the south-western Alpine fringe, indicating a mostly synchronous response of glaciers to LGM climatic changes across the region.
- For the larger glacial systems, the late LGM advance is manifested as a recessional moraine, inside the LGM maximum. Smaller glaciers, either appear to have reached the same frontal position during multiple advances, or the latest LGM advance overrode previously deposited moraines.
- Palaeoglacier ELAs in the Maritime Alps show considerable variability, from 1610 m a.s.l. for the north-facing Costa Ganola cirque glacier to 1980 m a.s.l. for the south-east facing Caramagne Glacier.
- Modelling received solar radiation suggests a strong influence of aspect and shading on the glacier ELAs that should be considered in any palaeoclimatic interpretations.
- The LGM ELA in the Maritime Alps was substantially higher than in the northern Apennines or the Corsican mountains. Assuming similar LGM temperatures, this ELA difference indicates substantially less humid climatic conditions in the Maritime Alps relative to these nearby sites.

CRediT authorship contribution statement

Lukas Rettig: Investigation, Writing - original draft, Visualization, Data curation. **Sarah Kamleitner:** Investigation, Writing - review & editing. **Paolo Mozzi:** Supervision, Investigation, Writing - review & editing. **Adriano Ribolini:** Conceptualization, Investigation, Writing - review & editing. **Susan Ivy-Ochs:** Investigation, Writing - review & editing. **Brice R. Rea:** Investigation, Writing - review & editing. **Giovanni Monegato:** Supervision, Writing - review & editing. **Marcus Christl:** Investigation, Writing - review & editing. **Matteo Spagnolo:** Supervision, Conceptualization, Funding acquisition.

Declaration of competing interest

The authors declare that they have no known competing financial interests or personal relationships that could have appeared to influence the work reported in this paper.

Data availability

Data will be made available on request.

Acknowledgements

The authors would like to thank Lucy Ashpitel for assisting with field work, Ewelina Brós for guidance in the sample preparation, and all members of the Laboratory of Ion Beam Physics at ETH Zurich for producing excellent exposure ages. This work received funding from the Royal Society (grant number: IEC/R2/202123) and through the RADIATE Transnational Access programme (proposal number: 22002973). Their financial and logistical support is gratefully acknowledged.

References

Akçar, N., Ivy-Ochs, S., Kubik, P.W., Schlüchter, C., 2011. Post-depositional impacts on 'Findlinge' (erratic boulders) and their implications for surface-exposure dating. Swiss J. Geosci. 104, 445–453. https://doi.org/10.1007/s00015-011-0088-7.

André, M.F., 2002. Rates of postglacial rock weathering on glacially scoured outcrops (Abisko–Riksgränsen area, 68°n). Geogr. Ann. Phys. Geogr. 84 (3–4), 139–150. https://doi.org/10.1111/j.0435-3676.2002.00168.x.

Balco, G., Stone, J.O., Lifton, N.A., Dunai, T.J., 2008. A complete and easily accessible means of calculating surface exposure ages or erosion rates from ^{10}Be and ^{26}Al measurements. Quat. Geochronol. 3 (3), 174–195. https://doi.org/10.1016/j.quageo.2007.12.001.

Balco, G., Briner, J., Finkel, R.C., Rayburn, J.A., Ridge, J.C., Schaefer, J.M., 2009. Regional beryllium-10 production rate calibration for late-glacial northeastern North America. Quat. Geochronol. 4 (2), 93–107. https://doi.org/10.1016/j.quageo.2008.09.001.

Baratto, A., Ferrarese, F., Meneghel, M., Sauro, U., 2003. La ricostruzione della glaciazione Wurmiana nel Gruppo del Monte Grappa (Prealpi Venete). In: Biancotti, A., Motta, M. (Eds.), Risposta dei processi geomorfologici alle variazioni ambientali. Brigati G., Genova, pp. 67–77.

Baroni, C., Pieruccini, P., Bini, M., Coltorti, M., Fantozzi, P.L., Guidobaldi, G., Nannini, D., Ribolini, A., Salvatore, M.C., 2015. Geomorphological and neotectonic map of the Apuan Alps (Tuscany, Italy). Geogr. Fis. Din. Quaternaria 38 (2), 201–227. https://doi.org/10.4461/GFDQ.2015.38.17.

Baroni, C., Guidobaldi, G., Salvatore, M.C., Christl, M., Ivy-Ochs, S., 2018. Last glacial maximum glaciers in the Northern Apennines reflect primarily the influence of southerly storm-tracks in the western Mediterranean. Quat. Sci. Rev. 197, 352–367. https://doi.org/10.1016/j.quascirev.2018.07.003.

Benn, D.I., Ballantyne, C.K., 2005. Palaeoclimatic reconstruction from Loch Lomond readvance glaciers in the west Drumochter Hills, Scotland. J. Quat. Sci. 20 (6), 577–592. https://doi.org/10.1002/jqs.925.

Benn, D.I., Hulton, N.R.J., 2010. An Excel™ spreadsheet program for reconstructing the surface profile of former mountain glaciers and ice caps. Comput. Geosci. 36 (5), 605–610. https://doi.org/10.1016/j.cageo.2009.09.016.

Bigot-Cormier, F., Braucher, R., Bourlès, D., Guglielmi, Y., Dubar, M., Stéphan, J.F., 2005. Chronological constraints on processes leading to large active landslides. Earth Planet Sci. Lett. 235 (1–2), 141–150. https://doi.org/10.1016/j.epsl.2005.03.012.

Bini, A., Buoncristiani, J.F., Couterrand, S., Ellwanger, D., Felber, M., Florineth, D., Graf, H.R., Keller, O., Kelly, M., Schlüchter, C., Schöneich, P., 2009. Die Schweiz während des letzteiszeitlichen Maximums (LGM), Bundesamt für Landestopographie swisstopo. Wabern.

Braakhekke, J., Ivy-Ochs, S., Monegato, G., Gianotti, F., Martin, S., Casale, S., Christl, M., 2020. Timing and flow pattern of the Orta glacier (European Alps) during the last glacial maximum. Boreas 49 (2), 315–332. https://doi.org/10.1111/bor.12427.

Chandler, B.M., Lukas, S., 2017. Reconstruction of Loch Lomond Stadial (Younger Dryas) glaciers on Ben More Coigach, north-west Scotland, and implications for reconstructing palaeoclimate using small ice masses. J. Quat. Sci. 32 (4), 475–492. https://doi.org/10.1002/jqs.2941.

Christl, M., Vockenhuber, C., Kubik, P.W., Wacker, L., Lachner, J., Alfimov, V., Synal, H. A., 2013. The ETH Zurich AMS facilities: performance parameters and reference materials. Nucl. Instrum. Methods Phys. Res. Sect. B Beam Interact. Mater. Atoms 294, 29–38. https://doi.org/10.1016/j.nimb.2012.03.004.

Clark, P.U., Dyke, A.S., Shakun, J.D., Carlson, A.E., Clark, J., Wohlfarth, B., Mitrovica, J. X., Hostetler, S.W., McCabe, A.M., 2009. The last glacial maximum. Science 325 (5941), 710–714. https://doi.org/10.1126/science.1172873.

Coleman, C.G., Carr, S.J., Parker, A.G., 2009. Modelling topoclimatic controls on palaeoglaciers: implications for inferring palaeoclimate from geomorphic evidence. Quat. Sci. Rev. 28 (3–4), 249–259. https://doi.org/10.1016/j.quascirev.2008.10.016.

Crespi, A., Brunetti, M., Lentini, G., Maugeri, M., 2018. 1961-1990 high-resolution monthly precipitation climatologies for Italy. Int. J. Climatol. 38 (2), 878–895. https://doi.org/10.1002/joc.5217.

Darnault, R., Rolland, Y., Braucher, R., Bourlès, D., Revel, M., Sanchez, G., Bouissou, S., 2012. Timing of the last deglaciation revealed by receding glaciers at the Alpine-scale: impact on mountain geomorphology. Quat. Sci. Rev. 31, 127–142. https://doi.org/10.1016/j.quascirev.2011.10.019.

Del Gobbo, C., Colucci, R.R., Monegato, G., Žebre, M., Giorgi, F., 2022. Atmosphere-cryosphere interactions at 21 ka BP in the European Alps. Clim. Past Discuss. https://doi.org/10.5194/cp-2022-43 [preprint], in review.

Ehlers, J., Gibbard, P.L., 2004. Quaternary Glaciations Extent and Chronology, Part I: Europe. Elsevier, Amsterdam.

Evans, I.S., Cox, N.J., 2005. Global variations of local asymmetry in glacier altitude: separation of north–south and east–west components. J. Glaciol. 51 (174), 469–482. https://doi.org/10.3189/172756505781829205.

Federici, P.R., Stefanini, M.C., 2001. Evidence and chronology of the Little ice age in the Argentera Massif (Italian Maritime Alps). Z. Gletscherkd. Glazialgeol. 37 (1), 35–48.

Federici, P.R., Pappalardo, M., Ribolini, A., 2003. Geomorphological Map of Maritime Alps Natural Park and Surroundings. Selca, Firenze.

Federici, P.R., Granger, D.E., Pappalardo, M., Ribolini, A., Spagnolo, M., Cyr, A.J., 2008. Exposure age dating and equilibrium line altitude reconstruction of an egesen moraine in the Maritime Alps, Italy. Boreas 37 (2), 245–253. https://doi.org/10.1111/j.1502-3885.2007.00018.x.

Federici, P.R., Pappalardo, M., 2010. Glacier retreat in the Maritime Alps area. Geogr. Ann. Phys. Geogr. 92 (3), 361–373. https://doi.org/10.1111/j.1468-0459.2010.00401.x.

Federici, P.R., Granger, D.E., Ribolini, A., Spagnolo, M., Pappalardo, M., Cyr, A.J., 2012. Last glacial maximum and the gschnitz stadial in the Maritime Alps according to ^{10}Be cosmogenic dating. Boreas 41 (2), 277–291. https://doi.org/10.1111/j.1502-3885.2011.00233.x.

Federici, P.R., Ribolini, A., Spagnolo, M., 2017. Glacial history of the Maritime Alps from the last glacial maximum to the Little ice age. Geological Society, London, Special Publications 433 (1), 137–159. https://doi.org/10.1144/SP433.9.

Florineth, D., Schlüchter, C., 2000. Alpine evidence for atmospheric circulation patterns in europe during the last glacial maximum. Quat. Res. 54 (3), 295–308. https://doi.org/10.1006/qres.2000.2169.

Forno, M.G., Gianotti, F., Racca, G., 2010. Significato paleoclimatico dei rapporti tra il glacialismo principale e quello tributario nella Bassa Valle della Dora Baltea. Il Quat. 23 (1), 105–124.

Fratianni, S., Acquaotta, F., 2017. The climate of Italy. In: Soldati, M., Marchetti, M. (Eds.), Landscapes and Landforms of Italy. Springer, Cham, pp. 29–38. https://doi.org/10.1007/978-3-319-26194-2_4.

Furbish, D.J., Andrews, J.T., 1984. The use of hypsometry to indicate long-term stability and response of valley glaciers to changes in mass transfer. J. Glaciol. 30 (105), 199–211. https://doi.org/10.3189/S0022143000005931.

Gaar, D., Graf, H.R., Preusser, F., 2019. New chronological constraints on the timing of Late Pleistocene glacier advances in northern Switzerland. E&G Quaternary Science Journal 68 (1), 53–73. https://doi.org/10.5194/egqsj-68-53-2019.

Gianotti, F., Forno, M.G., Ivy-Ochs, S., Kubik, P.W., 2008. New chronological and stratigraphical data on the Ivrea amphitheatre (Piedmont, NW Italy). Quat. Int. 190 (1), 123–135. https://doi.org/10.1016/j.quaint.2008.03.001.

Gianotti, F., Forno, M.G., Ivy-Ochs, S., Monegato, G., Pini, R., Ravazzi, C., 2015. Stratigraphy of the Ivrea morainic amphitheatre (NW Italy): an updated synthesis. Alpine and Mediterranean Quaternary 28, 29–58.

Giraudi, C., 2017. Climate evolution and forcing during the last 40 ka from the oscillations in Apennine glaciers and high mountain lakes, Italy. J. Quat. Sci. 32 (8), 1085–1098. https://doi.org/10.1002/jqs.2985.

Gribenski, N., Valla, P.G., Preusser, F., Roattino, T., Crouzet, C., Buoncristiani, J.F., 2021. Out-of-phase Late Pleistocene glacial maxima in the Western Alps reflect past changes in North Atlantic atmospheric circulation. Geology 49 (9), 1096–1101. https://doi.org/10.1130/G48688.1.

Heyman, J., Stroeven, A.P., Harbor, J.M., Caffee, M.W., 2011. Too young or too old: evaluating cosmogenic exposure dating based on an analysis of compiled boulder exposure ages. Earth Planet Sci. Lett. 302 (1–2), 71–80. https://doi.org/10.1016/j.epsl.2010.11.040.

Isotta, F.A., Frei, C., Weilguni, V., Perčec Tadić, M., Lassegues, P., Rudolf, B., Pavan, V., Cacciamani, C., Antolini, G., Ratto, S.M., Munari, M., Micheletti, S., Bonati, V., Lussana, C., Ronchi, C., Panettieri, E., Marigo, G., Vertačnik, G., 2014. The climate of daily precipitation in the Alps: development and analysis of a high-resolution grid dataset from pan-Alpine rain-gauge data. Int. J. Climatol. 34 (5), 1657–1675. https://doi.org/10.1002/joc.3794.

Ivy-Ochs, S., 1996. The Dating of Rock Surfaces Using in Situ Produced ^{10}Be, ^{26}Al and ^{36}Cl, with Examples from Antarctica and the Swiss Alps. ETH Zürich, p. 210. https://doi.org/10.3929/ethz-a-001772745. Ph.D. dissertation.

Ivy-Ochs, S., Schäfer, J., Kubik, P.W., Synal, H.A., Schlüchter, C., 2004. Timing of deglaciation on the northern Alpine foreland (Switzerland). Eclogae Geol. Helv. 97, 47–55. https://doi.org/10.1007/s00015-004-1110-0.

Ivy-Ochs, S., Kober, F., 2008. Surface exposure dating with cosmogenic nuclides. E&G Quaternary Science Journal 57 (1/2), 179–209. https://doi.org/10.3285/eg.57.1-2.7.

Ivy-Ochs, S., Lucchesi, S., Baggio, P., Fioraso, G., Gianotti, F., Monegato, G., Graf, A.A., Akçar, N., Christl, M., Carraro, F., Forno, M.G., Schlüchter, C., 2018. New geomorphological and chronological constraints for glacial deposits in the Rivoli-Avigliana end-moraine system and the lower Susa Valley (Western Alps, NW Italy). J. Quat. Sci. 33 (5), 550–562. https://doi.org/10.1002/jqs.3034.

Ivy-Ochs, S., Monegato, G., Reitner, J.M., 2022. The Alps: glacial landforms from the last glacial maximum. In: Palacios, D., Hughes, P.D., García-Ruiz, J.M., Andrés, N. (Eds.), European Glacial Landscapes: Maximum Extent of Glaciations. Elsevier, Amsterdam, pp. 449–460. https://doi.org/10.1016/B978-0-12-823498-3.00030-3.

Jóhannesson, T., 1986. The response time of glaciers in Iceland to changes in climate. Ann. Glaciol. 8, 100–101. https://doi.org/10.3189/S0260305500001233.

Jóhannesson, T., Raymond, C., Waddington, E., 1989. Time-scale for adjustment of glaciers to changes in mass balance. J. Glaciol. 35 (121), 355–369. https://doi.org/10.3189/S002214300000928X.

Jorda, M., Rosique, T., Évin, J., 2000. Données nouvelles sur l'âge du dernier maximum glaciaire dans les Alpes méridionales françaises. Comptes Rendus Acad. Sci. - Ser. IIA Earth Planet. Sci. 331 (3), 187–193. https://doi.org/10.1016/S1251-8050(00)01408-7.

Julian, M., 1980. Les Alpes maritimes franco-italiennes. Etude Géomorphologique. Aix-Marseille Université, p. 836. Ph.D. dissertation.

Kamleitner, S., Ivy-Ochs, S., Monegato, G., Gianotti, F., Akçar, N., Vockenhuber, C., Christl, M., Synal, H.A., 2022. The Ticino-Toce glacier system (Swiss-Italian Alps) in the framework of the alpine last glacial maximum. Quat. Sci. Rev. 279, 107400 https://doi.org/10.1016/j.quascirev.2022.107400.

Kamleitner, S., Ivy-Ochs, S., Manatschal, L., Akçar, N., Christl, M., Vockenhuber, C., Hajdas, I., Synal, H.A., 2023. Last Glacial Maximum glacier fluctuations on the northern Alpine foreland: geomorphological and chronological reconstructions from the Rhine and Reuss glacier systems. Geomorphology 423, 108548. https://doi.org/10.1016/j.geomorph.2022.108548.

Kirkbride, M.P., Winkler, S., 2012. Correlation of Late Quaternary moraines: impact of climate variability, glacier response, and chronological resolution. Quat. Sci. Rev. 46, 1–29. https://doi.org/10.1016/j.quascirev.2012.04.002.

Kłapyta, P., Mîndrescu, M., Zasadni, J., 2022. The impact of local topoclimatic factors on marginal Pleistocene glaciation in the Northern Romanian Carpathians. Catena 210, 105873. https://doi.org/10.1016/j.catena.2021.105873.

Kohl, C.P., Nishiizumi, K., 1992. Chemical isolation of quartz for measurement of in-situ-produced cosmogenic nuclides. Geochem. Cosmochim. Acta 56 (9), 3583–3587. https://doi.org/10.1016/0016-7037(92)90401-4.

Kronig, O., Ivy-Ochs, S., Hajdas, I., Christl, M., Wirsig, C., Schlüchter, C., 2018. Holocene evolution of the Triftje- and the Oberseegletscher (Swiss Alps) constrained with ^{10}Be exposure and radiocarbon dating. Swiss J. Geosci. 111, 117–131. https://doi.org/10.1007/s00015-017-0288-x.

Kuhlemann, J., Frisch, W., Székely, B., Dunkl, I., Danišik, M., Krumrei, I., 2005. Würmian maximum glaciation in Corsica. Austrian Journal of Earth Sciences 97, 68–81.

Kuhlemann, J., Rohling, E.J., Krumrei, I., Kubik, P., Ivy-Ochs, S., Kucera, M., 2008. Regional synthesis of mediterranean atmospheric circulation during the last glacial maximum. Science 321 (5894), 1338–1340. https://doi.org/10.1126/science.1157638.

Lal, D., 1991. Cosmic ray labeling of erosion surfaces: in situ nuclide production rates and erosion models. Earth Planet Sci. Lett. 104 (2–4), 424–439. https://doi.org/10.1016/0012-821X(91)90220-C.

Luetscher, M., Boch, R., Sodemann, H., Spötl, C., Cheng, H., Edwards, R.L., Frisia, S., Hof, F., Müller, W., 2015. North atlantic storm track changes during the last glacial maximum recorded by alpine speleothems. Nat. Commun. 6, 6344. https://doi.org/10.1038/ncomms7344.

Lukas, S., Graf, A., Coray, S., Schlüchter, C., 2012. Genesis, stability and preservation potential of large lateral moraines of Alpine valley glaciers - towards a unifying theory based on Findelengletscher, Switzerland. Quat. Sci. Rev. 38, 27–48. https://doi.org/10.1016/j.quascirev.2012.01.022.

Malaroda, R., Carraro, F., Dal Piaz, G., Franceschetti, B., Sturani, C., Zanella, E., 1970. Carta geologica del Massiccio dell'Argentera alla scala 1: 50.000. P. Mariotti, Pisa.

Marazzi, S., 2005. Atlante orografico delle Alpi. SOIUSA: suddivisione orografica internazionale unificata del sistema alpino. Priuli & Verlucca, Pavone Canavese, p. 416.

Mills, S.C., Grab, S.W., Rea, B.R., Carr, S.J., Farrow, A., 2012. Shifting westerlies and precipitation patterns during the Late Pleistocene in southern Africa determined using glacier reconstruction and mass balance modelling. Quat. Sci. Rev. 55, 145–159. https://doi.org/10.1016/j.quascirev.2012.08.012.

Mitchell, W.A., 1996. Significance of snowblow in the generation of loch lomond stadial (younger dryas) glaciers in the western pennines, northern england. J. Quat. Sci. 11 (3), 233–248. https://doi.org/10.1002/(SICI)1099-1417(199605/06)11:3<233::AID-JQS240>3.0.CO;2-Q.

Monegato, G., Ravazzi, C., Donegana, M., Pini, R., Calderoni, G., Wick, L., 2007. Evidence of a two-fold glacial advance during the last glacial maximum in the Tagliamento end moraine system (eastern Alps). Quat. Res. 68 (2), 284–302. https://doi.org/10.1016/j.yqres.2007.07.002.

Monegato, G., 2012. Local glaciers in the julian prealps (NE Italy) during the last glacial maximum. Alpine and Mediterranean Quaternary 25 (1), 5–14.

Monegato, G., Scardia, G., Hajdas, I., Rizzini, F., Piccin, A., 2017. The Alpine LGM in the boreal ice-sheets game. Sci. Rep. 7, 2078. https://doi.org/10.1038/s41598-017-02148-7.

Monegato, G., Kamleitner, S., Gianotti, F., Martin, S., Scapozza, C., Ivy-Ochs, S., 2022. The toce-ticino ice conveyor belts during the last glacial maximum. Alpine and Mediterranean Quaternary 35 (2), 119–134. https://doi.org/10.26382/AMQ.2022.07.

Musumeci, G., Ribolini, A., Spagnolo, M., 2003. The effects of late alpine tectonics in the morphology of the Argentera Massif (western Alps, Italy-France). Quat. Int. 101–102, 191–201. https://doi.org/10.1016/S1040-6182(02)00101-5.

Nishiizumi, K., Imamura, M., Caffee, M.W., Southon, J.R., Finkel, R.C., McAninch, J., 2007. Absolute calibration of ^{10}Be AMS standards. Nuclear Instruments & Methods in Physics Research Section B: Beam Interactions with Materials and Atoms 258 (2), 403–413. https://doi.org/10.1016/j.nimb.2007.01.297.

Nye, J.F., 1952. A method of calculating the thicknesses of the ice-sheets. Nature 169, 529–530. https://doi.org/10.1038/169529a0.

Nye, J.F., 1965. The flow of a Glacier in a channel of rectangular, elliptic or parabolic cross-section. J. Glaciol. 5 (41), 661–690. https://doi.org/10.3189/S0022143000018670.

Oerlemans, J., 2007. Estimating response times of Vadret da Morteratsch, Vadret da Palü, Briksdalsbreen and Nigardsbreen from their length records. J. Glaciol. 53 (182), 357–362. https://doi.org/10.3189/002214307783258387.

Ohmura, A., Kasser, P., Funk, M., 1992. Climate at the equilibrium line of glaciers. J. Glaciol. 38 (130), 397–411. https://doi.org/10.3189/S0022143000002276.

Ohmura, A., Boettcher, M., 2018. Climate on the equilibrium line altitudes of glaciers: theoretical background behind Ahlmann's P/T diagram. J. Glaciol. 64 (245), 489–505. https://doi.org/10.1017/jog.2018.41.

Oien, R.P., Rea, B.R., Spagnolo, M., Barr, I.D., Bingham, R.G., 2022. Testing the area-altitude balance ratio (AABR) and accumulation-area ratio (AAR) methods of calculating glacier equilibrium-line altitudes. J. Glaciol. 68 (268), 357–368. https://doi.org/10.1017/jog.2021.100.

Osmaston, H., 2005. Estimates of glacier equilibrium line altitudes by the Area×Altitude, the Area×Altitude balance ratio and the Area×Altitude balance index methods and their validation. Quat. Int. 138–139, 22–31. https://doi.org/10.1016/j.quaint.2005.02.004.

Paterson, W.S.B., 1994. The Physics of Glaciers, third ed. Pergamon/Elsevier, London.

Pellitero, R., Rea, B.R., Spagnolo, M., Bakke, J., Hughes, P., Ivy-Ochs, S., Lukas, S., Ribolini, A., 2015. A GIS tool for automatic calculation of glacier equilibrium-line altitudes. Comput. Geosci. 82, 55–62. https://doi.org/10.1016/j.cageo.2015.05.005.

Pellitero, R., Rea, B.R., Spagnolo, M., Bakke, J., Ivy-Ochs, S., Frew, C.R., Hughes, P., Ribolini, A., Lukas, S., Renssen, H., 2016. GlaRe, a GIS tool to reconstruct the 3D surface of palaeoglaciers. Comput. Geosci. 94, 77–85. https://doi.org/10.1016/j.cageo.2016.06.008.

Preusser, F., Blei, A., Graf, H., Schlüchter, C., 2007. Luminescence dating of Würmian (Weichselian) proglacial sediments from Switzerland: methodological aspects and stratigraphical conclusions. Boreas 36 (2), 130–142. https://doi.org/10.1111/j.1502-3885.2007.tb01187.x.

Putkonen, J., Swanson, T., 2003. Accuracy of cosmogenic ages for moraines. Quat. Res. 59 (2), 255–261. https://doi.org/10.1016/S0033-5894(03)00006-1.

Raper, S.C., Braithwaite, R.J., 2009. Glacier volume response time and its links to climate and topography based on a conceptual model of glacier hypsometry. Cryosphere 3 (2), 183–194. https://doi.org/10.5194/tc-3-183-2009.

Ravazzi, C., Badino, F., Marsetti, D., Patera, G., Reimer, P.J., 2012. Glacial to paraglacial history and forest recovery in the Oglio glacier system (Italian Alps) between 26 and 15 ka cal BP. Quat. Sci. Rev. 58, 146–161. https://doi.org/10.1016/j.quascirev.2012.10.017.

Rea, B.R., 2009. Defining modern day Area-Altitude Balance Ratios (AABRs) and their use in glacier-climate reconstructions. Quat. Sci. Rev. 28 (3–4), 237–248. https://doi.org/10.1016/j.quascirev.2008.10.011.

Rea, B.R., Pellitero, R., Spagnolo, M., Hughes, P., Ivy-Ochs, S., Renssen, H., Ribolini, A., Bakke, J., Lukas, S., Braithwaite, R.J., 2020. Atmospheric circulation over europe during the younger dryas. Sci. Adv. 6 (50), eaba4844 https://doi.org/10.1126/sciadv.aba4844.

Reber, R., Akçar, N., Ivy-Ochs, S., Tikhomirov, D., Burkhalter, R., Zahno, C., Lüthold, A., Kubik, P.W., Vockenhuber, C., Schlüchter, C., 2014. Timing of retreat of the reuss glacier (Switzerland) at the end of the last glacial maximum. Swiss J. Geosci. 107, 293–307. https://doi.org/10.1007/s00015-014-0169-5.

Rettig, L., Monegato, G., Mozzi, P., Žebre, M., Casetta, L., Fernetti, M., Colucci, R.R., 2021. The Pleistocene evolution and reconstruction of LGM and late glacial paleoglaciers of the silisia valley and mount raut (carnic prealps, NE-Italy). Alpine and Mediterranean Quaternary 34 (2), 277–290.

Rettig, L., Monegato, G., Spagnolo, M., Hajdas, I., Mozzi, P., 2023. The equilibrium line altitude of isolated glaciers during the last glacial maximum–new insights from the geomorphological record of the Monte cavallo group (south-eastern European Alps). Catena 229, 107187. https://doi.org/10.1016/j.catena.2023.107187.

Reuther, A.U., Fiebig, M., Ivy-Ochs, S., Kubik, P.W., Reitner, J.M., Jerz, H., Heine, K., 2011. Deglaciation of a large piedmont lobe glacier in comparison with a small mountain glacier – new insight from surface exposure dating. Two studies from SE Germany. E&G Quaternary Science Journal 60 (2/3), 248–269. https://doi.org/10.3285/eg.60.2-3.03.

Ribolini, A., 2000. Relief distribution, morphology and cenozoic differential uplift in the Argentera Massif (French-Italian Alps). Z. Geomorphol. 44 (3), 363–378. https://doi.org/10.1127/zfg/44/2000/363.

Ribolini, A., Spagnolo, M., 2008. Drainage network geometry versus tectonics in the Argentera Massif (French–Italian Alps). Geomorphology 93 (3–4), 253–266. https://doi.org/10.1016/j.geomorph.2007.02.016.

Ribolini, A., Spagnolo, M., Cyr, A.J., Federici, P.R., 2022a. Last glacial maximum and early deglaciation in the Stura Valley, southwestern European Alps. Quat. Sci. Rev. 295, 107770 https://doi.org/10.1016/j.quascirev.2022.107770.

Ribolini, A., Spagnolo, M., Giraudi, C., 2022b. The Italian mountains: glacial landforms from the Last Glacial Maximum. In: Palacios, D., Hughes, P.D., García-Ruiz, J.M., Andrés, N. (Eds.), European Glacial Landscapes: Maximum Extent of Glaciations. Elsevier, Amsterdam, pp. 481–486. https://doi.org/10.1016/B978-0-12-823498-3.00022-4.

Roattino, T., Crouzet, C., Vassallo, R., Buoncristiani, J.F., Carcaillet, J., Gribenski, N., Valla, P.G., 2022. Paleogeographical reconstruction of the western French Alps foreland during the last glacial maximum using cosmogenic exposure dating. Quat. Res. 111, 68–83. https://doi.org/10.1017/qua.2022.25.

Rolland, Y., Darnault, R., Braucher, R., Bourlès, D., Petit, C., Bouissou, S., ASTER team, 2020. Deglaciation history at the Alpine-Mediterranean transition (Argentera-Mercantour, SW Alps) from ^{10}Be dating of moraines and glacially polished bedrock. Earth Surf. Process. Landforms 45 (2), 393–410. https://doi.org/10.1002/esp.4740.

Schilling, D.H., Hollin, J.T., 1981. Numerical reconstructions of valley glaciers and small ice caps. In: Denton, G.H., Hughes, T.J. (Eds.), The Last Great Ice Sheets. Wiley, New York, pp. 207–220.

Seguinot, J., Ivy-Ochs, S., Jouvet, G., Huss, M., Funk, M., Preusser, F., 2018. Modelling last glacial cycle ice dynamics in the Alps. Cryosphere 12 (10), 3265–3285. https://doi.org/10.5194/tc-12-3265-2018.

Spagnolo, M., Ribolini, A., 2019. Glacier extent and climate in the Maritime Alps during the younger dryas. Palaeogeogr. Palaeoclimatol. Palaeoecol. 536, 109400 https://doi.org/10.1016/j.palaeo.2019.109400.

Spinicci, A., 1994. Lineamenti Geomorfologici Dell'alta Valle Vermenagna. Unpublished Master Thesis, University of Pisa.

Spötl, C., Koltai, G., Jarosch, A.H., Cheng, H., 2021. Increased autumn and winter precipitation during the last glacial maximum in the European Alps. Nat. Commun. 12, 1839. https://doi.org/10.1038/s41467-021-22090-7.

Stone, J.O., 2000. Air pressure and cosmogenic isotope production. J. Geophys. Res. Solid Earth 105 (B10), 23753–23759. https://doi.org/10.1029/2000JB900181.

Ye, S., Cuzzone, J.K., Marcott, S.A., Licciardi, J.M., Ward, D.J., Heyman, J., Quinn, D.P., 2023. A quantitative assessment of snow shielding effects on surface exposure dating from a western North American ^{10}Be data compilation. Quat. Geochronol. 76, 101440 https://doi.org/10.1016/j.quageo.2023.101440.